Stem Cell Reports
Resource
OPEN ACCESS

Integrated Genomic Analysis of Diverse Induced Pluripotent Stem Cells from the Progenitor Cell Biology Consortium

Nathan Salomonis,[1,16] Phillip J. Dexheimer,[1,16] Larsson Omberg,[2] Robin Schroll,[3] Stacy Bush,[3] Jeffrey Huo,[4,5] Lynn Schriml,[6] Shannan Ho Sui,[7,8] Mehdi Keddache,[9] Christopher Mayhew,[10] Shiva Kumar Shanmukhappa,[11] James Wells,[10] Kenneth Daily,[2] Shane Hubler,[2] Yuliang Wang,[12] Elias Zambidis,[4,5] Adam Margolin,[2,12] Winston Hide,[7,8,13] Antonis K. Hatzopoulos,[14] Punam Malik,[3] Jose A. Cancelas,[3,15] Bruce J. Aronow,[1,17] and Carolyn Lutzko[3,15,17,*]

[1]Department of Biomedical Informatics, Cincinnati Children's Hospital, Cincinnati, OH 45229, USA
[2]Sage Bionetworks, Seattle, WA 98109, USA
[3]Division of Experimental Hematology and Cancer Biology, Cincinnati Children's Hospital, Cincinnati, OH 45229, USA
[4]Institute for Cell Engineering, Johns Hopkins University School of Medicine, Baltimore, MD 21205, USA
[5]Division of Pediatric Oncology, Sidney Kimmel Comprehensive Cancer Center at Johns Hopkins, Baltimore, MD 21205, USA
[6]Department of Epidemiology and Public Health, Institute for Genome Sciences, University of Maryland School of Medicine, Baltimore, MD 21201, USA
[7]Department of Biostatistics, Harvard T.H. Chan School of Public Health, Boston, MA 02115, USA
[8]Harvard Stem Cell Institute, Cambridge, MA 02138, USA
[9]Division of Human Genetics
[10]Division of Developmental Biology
[11]Division of Pathology
Cincinnati Children's Hospital, Cincinnati, OH 45229, USA
[12]Computational Biology Program, Oregon Health & Science University, Portland, OR 97239, USA
[13]Sheffield Institute for Translational Neuroscience, University of Sheffield, Sheffield S10 2HQ, UK
[14]Division of Cardiovascular Medicine, Departments of Medicine and Cell and Developmental Biology, Vanderbilt University, Nashville, TN 37232, USA
[15]Hoxworth Blood Center, University of Cincinnati, Cincinnati, OH 45229, USA
[16]Co-first author
[17]Co-senior author
*Correspondence: carolyn.lutzko@cchmc.org
http://dx.doi.org/10.1016/j.stemcr.2016.05.006

SUMMARY

The rigorous characterization of distinct induced pluripotent stem cells (iPSC) derived from multiple reprogramming technologies, somatic sources, and donors is required to understand potential sources of variability and downstream potential. To achieve this goal, the Progenitor Cell Biology Consortium performed comprehensive experimental and genomic analyses of 58 iPSC from ten laboratories generated using a variety of reprogramming genes, vectors, and cells. Associated global molecular characterization studies identified functionally informative correlations in gene expression, DNA methylation, and/or copy-number variation among key developmental and oncogenic regulators as a result of donor, sex, line stability, reprogramming technology, and cell of origin. Furthermore, X-chromosome inactivation in PSC produced highly correlated differences in teratoma-lineage staining and regulator expression upon differentiation. All experimental results, and raw, processed, and metadata from these analyses, including powerful tools, are interactively accessible from a new online portal at https://www.synapse.org to serve as a reusable resource for the stem cell community.

INTRODUCTION

Pluripotent stem cells (PSC) have been used to study human development, model disease, and generate cellular tools for regenerative medicine. Human embryonic stem cells (hESC) have been considered the functional, genetic, and epigenetic gold standard in the field (Thomson et al., 1998). Methods of somatic cell reprogramming to generate induced PSC (iPSC) (Takahashi and Yamanaka, 2006) are continually being improved and have enabled the generation of iPSC using a variety of somatic cell sources, gene combinations, and methodologies. However, due to the intensive resources required for iPSC generation and characterization, direct comparisons of iPSC generated using a wide range of technologies and cell sources from multiple independent laboratories have rarely been performed, making it unclear whether all methodologies produce iPSC with a similar quality and stability.

A variety of studies have compared the expression profiles, pluripotentiality, and genetic and epigenetic stability of hESC and iPSC including lines generated using different strategies, distinct parental somatic cell types, or reprogramming methods (Bock et al., 2011; International Stem Cell Initiative et al., 2007; Müller et al., 2011; Rouhani et al., 2014; Schlaeger et al., 2015). However, these have been limited to a few variables, have multiple methods or laboratories collecting and processing samples, and typically employ a single genomics platform. "Multi-omics" analyses have proved to be essential in deciphering complex gene regulatory programs, as demonstrated by analyses of iPSC reprogramming transitional states (Clancy et al., 2014; Lee et al., 2014; Tonge et al., 2014).

The Progenitor Cell Biology Consortium (PCBC) of the National Heart, Lung and Blood Institute was founded to study iPSC reprogramming and differentiation and develop strategies to address the challenges presented by the transplantation of these cells. These questions include, but are not limited to: (1) Do iPSC consistently generate all three germ layers? (2) How prevalent is copy-number variation (CNV) in iPSC generated using different reprogramming methodologies? (3) Do different reprogramming methods affect global methylation, gene, splicing and microRNA (miRNA) expression profiles? (4) Can aberrant PSC gene regulation be identified on a global basis? (5) How do variables such as X-chromosome inactivation (XCI) affect iPSC quality, stability, and differentiation potential? To advance these goals, the PCBC developed a Central Cell Characterization Core and Bioinformatics Core to perform standardized and comprehensive characterization of iPSC generated using different somatic cell sources, methodologies, and vectors. The characterized iPSC are being made available through WiCell Research Institute.

Using integrative analyses across genomic analysis platforms, we present comparative results on phenotype, genetics, epigenetics, and gene regulation for a diverse panel of iPSC and hESC. Standardized methods and strict control of reagents during cell culture, sample collection, and assay performance were used to evaluate the innate potential and limitations of these cells with fewer confounding factors. Our use of this uniform analytical methodology allowed us to discover candidate regulators of the fate of reprogrammed cells. To maximize the utility of this resource, we developed an interactive open data portal for access to the raw data, metadata, results, and protocols from these experiments for further analysis (https://www.synapse.org/PCBC).

RESULTS

Study Design and Synapse Analysis Portal

An overview of the study is presented in Figure 1. The evaluation of iPSC from multiple laboratories and methodologies required highly structured cell-line annotations and well-documented protocols to make comprehensive comparisons possible. Metadata standards were developed to capture the origin of each line, starting cell type, donor demographics, and reprogramming parameters (derivation method, vector type, reprogramming genes, culture conditions). These metadata were provided by the originating laboratory and confirmed and augmented with in vitro genetic and experimental characterization of the line. RNA sequencing (RNA-seq) was performed at an acceptable depth to facilitate accurate gene-expression quantification (Supplemental Experimental Procedures). To facilitate use of the protocols, genomic analyses, and metadata produced through this effort, we developed a sophisticated interactive data portal, the interface of which is exemplified in Figure 1. In addition to integrated provenance annotations for every raw data file, script, or processed result file, data can be queried through an interactive heatmap viewer that displays and inter-relates gene expression, DNA methylation, and miRNA expression for queried genes, pathways, and gene signatures produced in the analyses described here. These signatures have been further propagated into ToppGene (Chen et al., 2009) for interactive queries. Synapse IDs are included to access the resources, data, metadata, ontologies, and other information through the Synapse online repository.

Screening of Lines

The data from the first 64 lines (58 iPSC and 6 hESC) enrolled in the study are presented here with their characteristics outlined in Figure 2A (details in syn2767694). All lines completed a standardized screen to ensure they met a basic set of criteria. This included self-renewal in defined feeder-free conditions, expression of markers of pluripotency and a lack of expression of markers of differentiation, a normal karyotype, and the ability to grow sufficient quantities of cells for the analyses (Tables S2 and S3; Figure S1). Overall, 6 hESC and 35 iPSC (64%) met these criteria and 23 iPSC did not (36%) (Table S4). Abnormal karyotypes were observed in seven lines (Table S5), with karyotypes for all lines available (syn2679104). The most consistent flow cytometry anomalies were TRA-1-81 and TRA-1-60 below 90% or an increase in SSEA-1 above 5% (Figure 2B). Due to contamination, difficulty in expanding cells, and/or abnormal karyotype, not all lines were included in functional pluripotency assays.

Pluripotency Analysis

Pluripotency was evaluated in a teratoma assay on 49 lines. Forty-six of the lines met the screening criteria outlined in Table S3 and 45 of these lines generated teratomas. Three lines did not meet the PSC screening criteria with decreased expression of self-renewal markers and increased differentiation in culture (SC12-021, SC12-023, and SC14-082), and all three successfully generated teratomas. All teratomas were scored by a clinical pathologist, and representatives of all three embryonic germ layers were identified in all tumors (detailed information is available at Synapse syn2882785). We performed immunostaining analysis on teratomas from a subset of lines to confirm pluripotency (muscle-specific actin [MSA], neurofilament, and α-fetoprotein) and OCT4 to evaluate the presence of undifferentiated PSC (Figure S1). This included two lines that did not meet the screening criteria and independent iPSC from the same donor as controls (Table S7), and three teratomas that

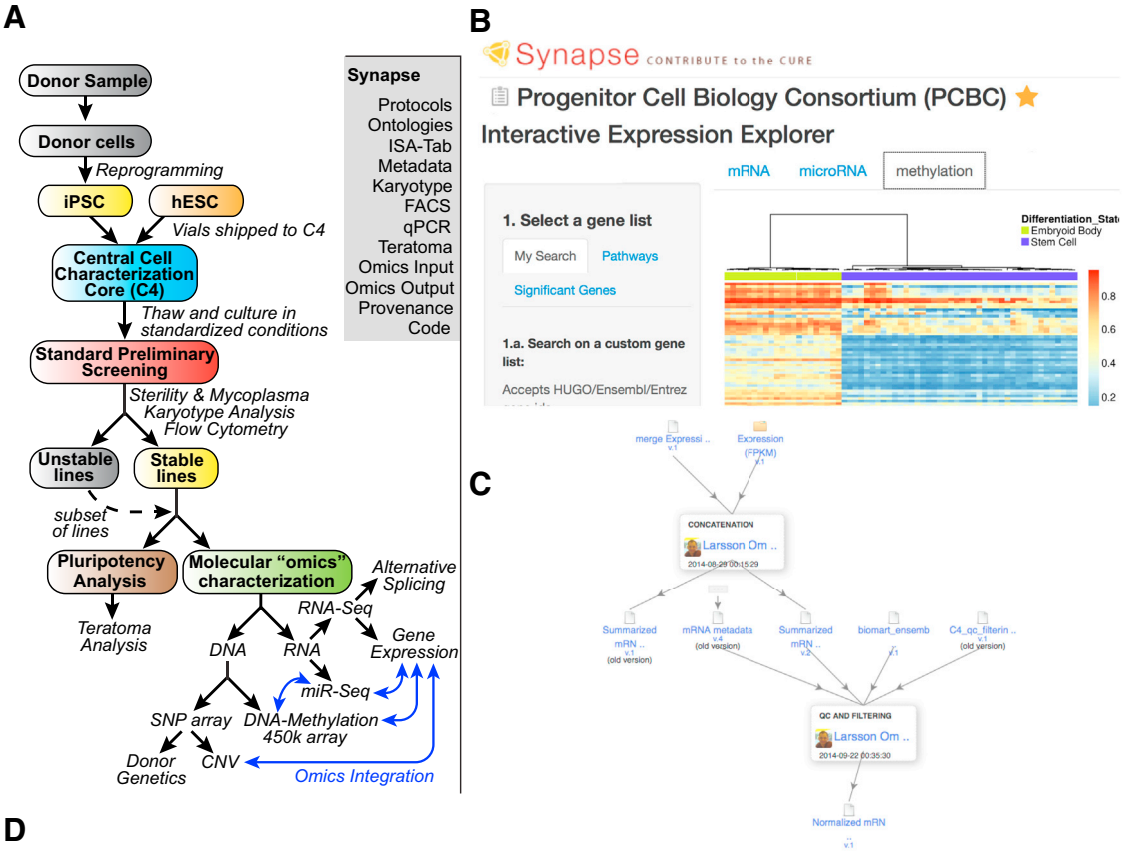

Figure 1. Study Design and Synapse Results Portal

(A) Overview of study design and data deposited online in Synapse. FACS, fluorescence-activated cell sorting; ISA-Tab, investigation/study/assay tab-delimited format.

(B) Synapse heatmap viewer displaying probes corresponding to EB-induced transcription factors and associated DNA-methylation levels to visually detected outliers in PSC.

(C) Provenance for the creation of normalized gene-expression values, associated scripts, quality control, metadata, and annotations.

(D) Gene-enrichment analysis in ToppGene displaying top-ranking PCBC stem cell signatures.

had regions histopathologically classified as poorly differentiated as well as independent teratomas generated from the same lines (Table S8). The immunostaining confirmed pluripotency in all tumors (Figure S1). OCT4 staining was observed in one teratoma with a poorly differentiated region (SC12-034), although other teratomas from this line were fully differentiated and did not have OCT-4-stained regions. Two teratomas from other lines (SC11-014 and SC11-0013) with poorly differentiated regions did not have OCT4 immunoreactivity, although we did not have adjacent sections for staining (Table S8).

Evaluation of CNV Changes in iPSC

Genetic stability was evaluated between independent lines with common donors by CNV SNP microarrays. Although two SNP genotyping arrays were used, all lines derived from a single donor were run on the same platform (see Experimental Procedures). Variations were observed in all lines and on all chromosomes (Figure S2). Excluding human leukocyte antigen-associated regions, 724 non-benign or clinically significant CNV from 529 unique genomic loci were identified (syn3105726). Although not significant, lines reprogrammed with integrating vectors trended

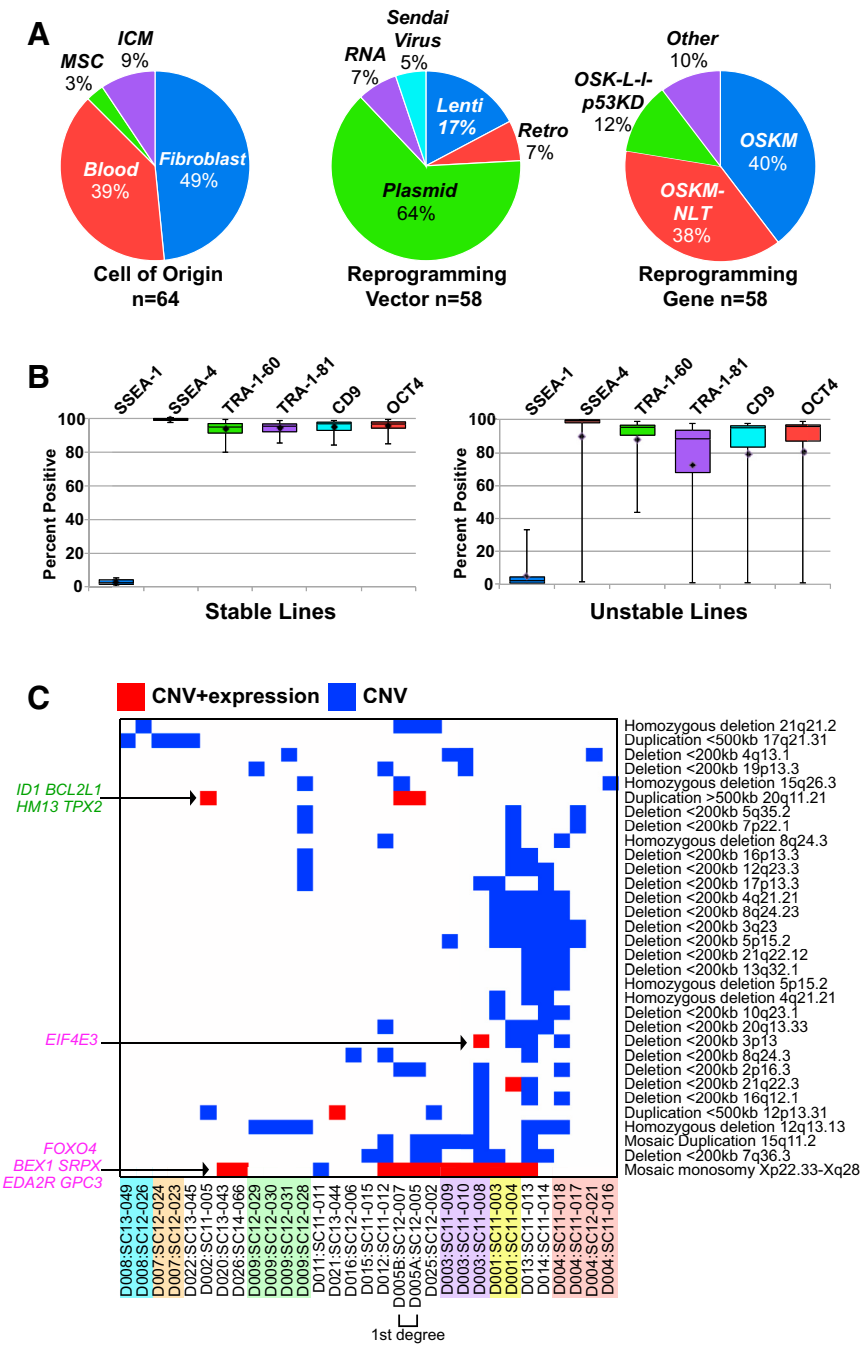

Figure 2. iPSC Line Characteristics, Flow Cytometry Analysis, and CNV Accumulation

(A) Reprogramming variables for: originating cell type (left), reprogramming vector (middle), and gene combination (right). Reprogramming gene combinations: OSKM is composed of *POU5F1* (also known as *OCT4*), *SOX2*, *KLF4*, and c-*MYC*; OSK-L-l-p53KD includes *LIN28A* and *TP53* knockdown and *l-MYC* instead of c-*MYC*; OSKM-NLT includes *NANOG*, *LIN28A*, and SV40 large T antigen. ICM, inner cell mass; MSC, mesenchymal stem cell.

(B) Flow cytometry analysis classified iPSC as stable (n = 41) or unstable (n = 11). Boxes represent the first and third quartiles, whiskers show the complete range, and the horizontal line is the median.

(C) Commonly observed CNV predicted as non-benign or clinically significant and observed from at least three independent genetic donors are listed on the right and shown as a heatmap (blue). Red cells indicate that CNV overlaps genes with concordant expression differences. Concordant genes with known function are labeled on the left, with previously identified tumor-suppressor genes in purple and cell-growth-promoting and oncogenesis-promoting genes in green. Lines from the same donor are highlighted in the same color.

toward a higher frequency of clinically significant CNV (58%) compared with non-integrating vectors (41%).

Our study included different iPSC generated from the same donor sample and reprogramming methods, thereby enabling the direct evaluation of the CNV present in the donor versus those induced during reprogramming and culture. We observed CNV that were specific to the donor, and others present among multiple genetically distinct iPSC (Figure S2). We identified lines generated from the same donor samples that had variable CNV (Table S6), with some donors having higher frequencies of CNV than others (such as D001, 2, 3, 4, and 9).

We discovered 102 non-benign CNV shared by at least two distinct donors, with 83 of these CNV variably present in two or more distinct samples from a common donor. Two donors (D004 and D003) were solely responsible for 46 of these CNV, while 26 were recurrent among multiple donors (Figure S2C). A more stringent analysis considering

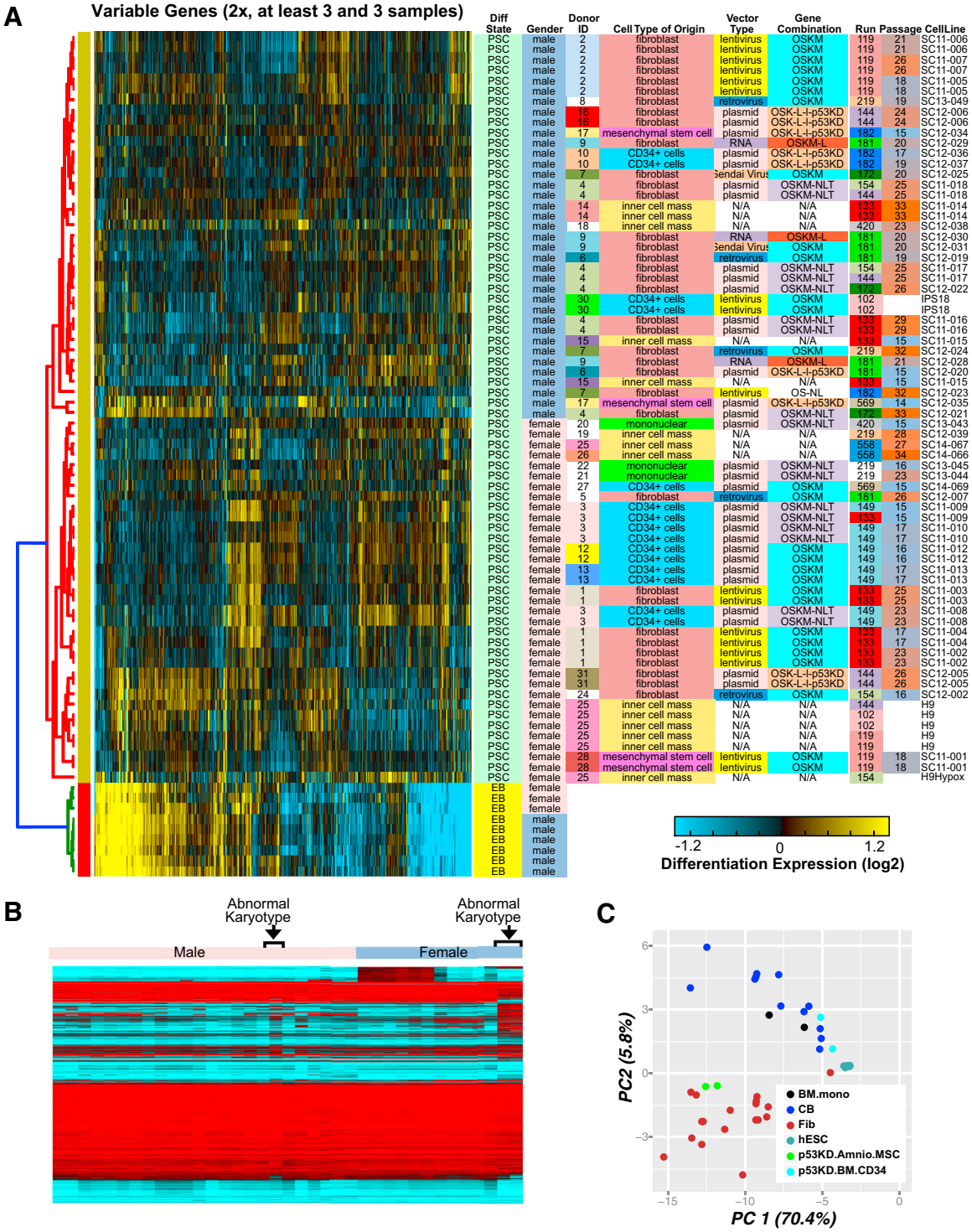

Figure 3. Global Gene Expression and Methylation Variation between iPSC

(A) Hierarchical clustering of the most variable genes observed among iPSC and hESC (n = 1,031). These genes were chosen by selecting the reliably expressed genes (n = 9,670) that varied at least 2-fold between six or more samples and correlated ($\rho > 0.5$) to the expression of at least ten other genes (AltAnalyze, Predict Groups analysis). Yellow indicates upregulated and blue indicates downregulated genes.

(legend continued on next page)

CNV shared among at least three donors identified a set of 31 frequently affected genomic loci, suggesting that they occurred during iPSC reprogramming or that the starting samples were mosaic (Abyzov et al., 2012; McConnell et al., 2013; Young et al., 2012) (Figure 2).

Comparison of the CNV and RNA-seq data identified 19 non-benign and clinically significant CNV that overlap with differentially expressed genes in a manner consistent with the detected duplication or deletion (syn2731183) (Figure 2C). This included 88 downregulated genes in deleted regions, 79 of which correspond to the frequently observed X-chromosome mosaic monosomy. Among 26 upregulated genes in duplicated regions, a duplication of 20q11.21 corresponded to the upregulation of nine overlapping genes, including four (*ID1*, *BCL2L1*, *HM13*, and *TPX2*) previously shown to promote hESC survival or oncogenic potential (Nguyen et al., 2014). We also found compatible regulation of the cancer susceptibility genes *FYN* (6q21 duplication), *ERCC2* (19q13.32 duplication), and *NIN* (14q22.1 duplication), as well as the tumor-suppressor genes *FOXO4*, *BEX1*, *SRPX*, *EDA2R*, *GPC3* (X monosomy), *ING2* (4q35.1 deletion), and *EIF4E3* (3p13 deletion) (Osborne et al., 2013). These results are consistent with these CNV conferring a survival or proliferative advantage.

Global Expression and Methylation Analysis of PSC

To understand the molecular determinants of PSC quality as a function of reprogramming method and somatic cell origin, we performed mRNA, miRNA, and methylation profiling on iPSC and hESC with profiles from hESC-derived embryoid bodies (EB) as a control.

Relative to EB, hESC and iPSC were largely indistinguishable from each other at the global gene-expression level by both hierarchical clustering and principal component analysis (PCA) (syn3107554). Greater variability was observed from analogous DNA methylation and miRNA profiles (Figure S3). However, restricting the analysis to genes with varying expression only in PSC identifies donor, sex, reprogramming technology, and originating laboratory as the major driving covariates by hierarchical clustering (Figure 3A). These differences did not clearly associate with the passage number of the profiled PSC. Of interest, H9 cells (D025) analyzed greater than ten passages apart displayed a highly variable signature with the higher passage more similar to EB. Likewise, one of two mesenchymal stem cell-derived iPSC from the same donor and laboratory (D017) exhibited a similar EB-like signature. Neither the D017 nor the H9 samples displayed apparent global DNA methylation differences, demonstrating the utility of distinct genomic platforms in assessing PSC quality (Figure S3).

To identify differences associated with major cell-line variables, we performed all possible pairwise comparisons from each metadata category for gene expression, splicing, miRNA, and DNA methylation (syn3094629). We identified 355 differentially expressed genes from these comparisons and 3,451 differential methylated DNA probes. As expected, laboratory of origin accounted for the largest number of differences, likely because several iPSC derivation protocols and cell types of origin were largely unique to a single laboratory (e.g., RNA-based reprogramming, stromal priming) and could therefore mask handling or other technical differences between laboratories. The major distinguishing reprogramming variables from the methylation analyses were cell type of origin (1,427 probes), method of reprogramming (1,346 probes), and sex (520 probes). Clustering of these methylation profiles readily distinguished lines based on both sex and abnormal karyotypes (Figure 3B), while PCA segregated samples based on cell of origin (Figure 3C). Although these samples consistently segregated by cell of origin independently of the donor sex, these differences could not be directly attributed to blood and fibroblast somatic methylation profile differences (data not shown).

To examine the impact on possible pathways, we looked at the enrichment of our discovered reprogramming regulated genes among gene ontology (GO) terms for each of the different measurement platforms (Figure 4A). The most prominent pathway level effects were found in the methylation comparisons with hESC for a wide array of biological comparisons and tested reprogramming variables. We observed consistent regulation of inflammatory and immune response, ion homeostasis, and regulation of cell proliferation gene sets, particularly among all iPSC compared with hESC, among the different profiling technologies.

To determine whether differential methylation might be a source of observed gene-expression differences, we compared the expression profiles of these differentially regulated genes and probes, based on common gene

Expression is shown relative to day 17 EB derived from multiple hESC (median-based normalization applied to preferentially identify PSC variance). Selected metadata associated with each cell line are shown on the right, with identical terms in each column sharing a color.
(B) Expression clustering of all CpG methylation probes on the X chromosome, with blue indicating hypo- and red hypermethylation. Lines with an abnormal karyotype are indicated.
(C) Principal component analysis of all differentially methylated probes for all evaluated PSC lines, colored according to cell of origin. BM.mono, bone marrow-derived monocytes; CB, umbilical cord blood; Fib, fibroblasts; Amnio.MSC, amniotic fluid-derived mesenchymal stem cells; BM.CD34, bone marrow-derived CD-34^{+} cells; p53KD, OSKL-l-p53KD reprogramming vector.

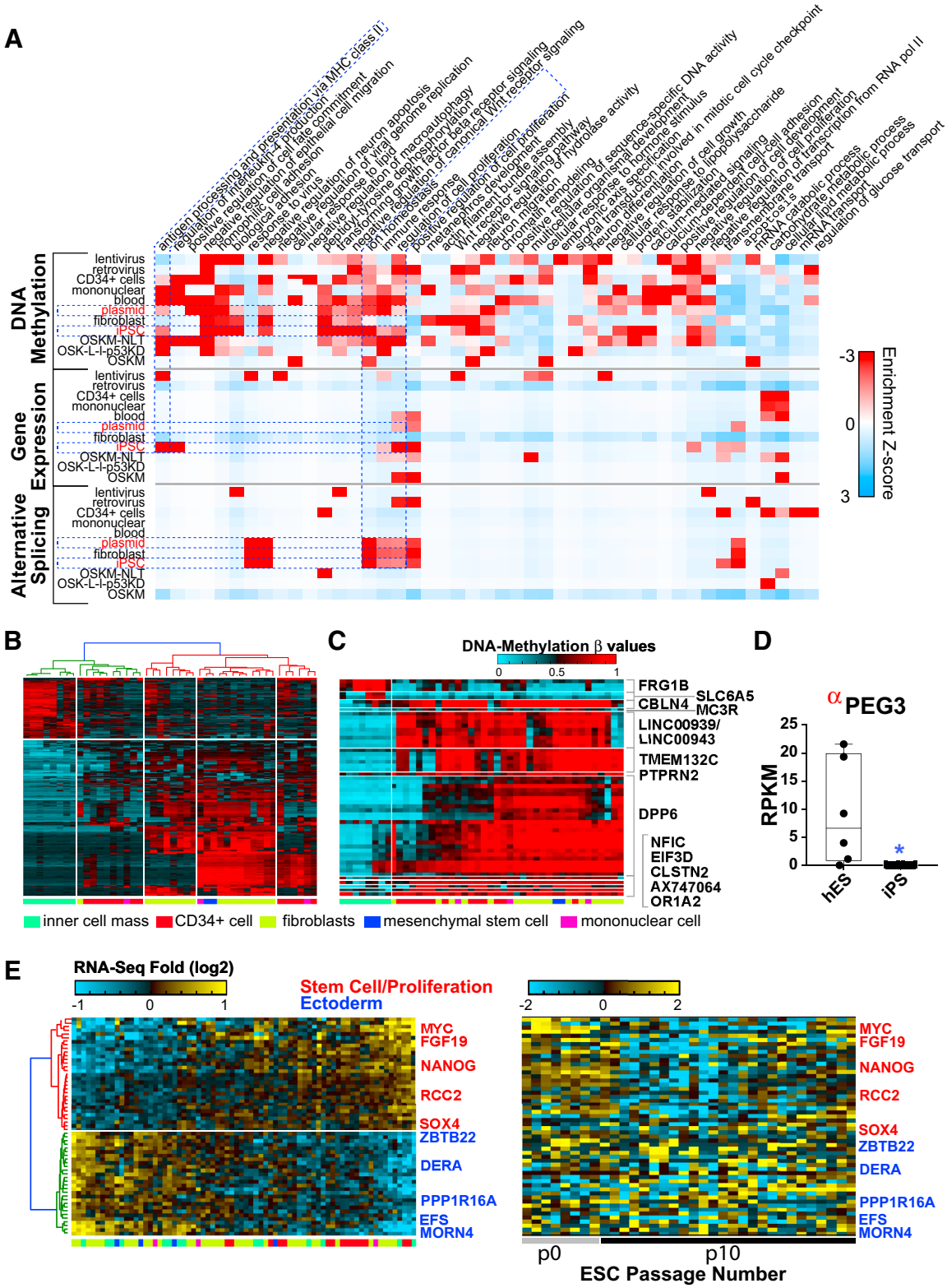

(legend on next page)

annotations (e.g., promoter, body, or UTR location of the probe). This analysis indicates that ~21% of all differentially methylated probes correspond to gene-expression changes in the PSC, while ~43% of all differentially expressed genes appear to be due to underlying differential DNA methylation (Pearson $\rho < -0.5$). Only negative correlations were considered from these analyses. Taken together, these data suggest that while iPSC are largely similar to hESC at the level of gene expression, observed differences are frequently correlated with changes in DNA methylation.

Comparison of hESC and iPSC

Among DNA-methylation profiles, comparison of all iPSC to hESC yielded 180 differentially methylated sites, with 52% of these anti-correlated with gene expression (n = 93). A more relaxed analysis (non-adjusted moderated t test $p < 0.05$) of unique donor samples indicated that methylation probes largely segregated by donor and cell of origin when subjected to hierarchical clustering (Figure 4B). In agreement with previously published studies, *DPP6*, *TMEM132C*, and *PTPRT* were among the most differentially methylated loci between iPSC and hESC (Figure 4C). In addition, we found that several interesting gene loci were hypomethylated (*FRG1B*, *SLC6A5*) and hypermethylated (*PTPRN2*, *LINC00939*, *CBLN4*, *MC3R*, *NFIC*, *EIF3D*, *CLSTN2*, *AX747064*, and *OR1A2*) in iPSC. Genes hypermethylated in iPSC were associated with neuronal differentiation and genomic targets of the polycomb repressive complex 2 (PRC2) (ToppGene). The most highly differentially expressed iPSC versus hESC gene, the paternally imprinted *PEG3*, was also anti-correlated with DNA-methylation probes (Pearson $\rho < -0.98$) (Figure 4D).

A close examination of the expression of core pluripotency factors across all PSC identified a large number of genes correlated and anti-correlated with *NANOG* and *MYC* (Figure 4E). Genes coexpressed with *NANOG* and *MYC* were enriched in negative regulators of differentiation, stem cell maintenance, and positive regulation of cell proliferation, while anti-correlated genes were enriched in experimentally observed ectoderm differentiation upregulated genes (ToppGene). To test whether these differences could be related to PSC quality and increased passaging, we compared the expression of these same genes with hESC from a previously described single-cell RNA-seq dataset (Figure 4E) (Yan et al., 2013). Clustering of both early (passage 0) and late (passage 10) single-cell hESC confirmed that *NANOG* and *MYC* high lines were most similar to early-passage hESC.

Genomic Impact of Reprogramming Technology, Cell of Origin, and iPSC Stability

Among the 64 lines evaluated, 41 underwent genomics characterization, with five unstable lines included as controls. These 46 lines comprised five cell-of-origin groups, five reprogramming vector types, and five distinct gene combinations. Comprehensive pairwise comparisons of all metadata categories across each genomics platform highlighted a large number of genes (syn3106206), splicing variants (syn3106266), methylation probes (syn3106255), and miRNAs (syn3106244) strongly associated with one or more of these variables (Figure 5). To our knowledge, few of these molecular differences have previously been reported. Many of the most significant differences were observed among differentially methylated probes (Figures 5A and S4A). For example, *SOX2* was hypermethylated in retroviral lines relative to all hESC and nearly all iPSC. Reciprocal differences in gene expression were frequently observed for these and many other differentially methylated genes.

For all genomic analyses, the small number of unique donors available for certain reprogramming methods limited the power of our analysis. However, the availability of a small number of iPSC derived from the same donor with different methods provides additional confirmation of our findings. For example, differentially expressed

Figure 4. Global Reprogramming Impact on Pathways in PSC

(A) Pathway-level impact of reprogramming methodology or initiating cell type as compared with hESC, based on statistically enriched GO terms for each comparison and profiling technology. Red indicates higher *Z* scores, corresponding to lower GO-Elite enrichment p values. Dashed blue lines indicate common regulated pathways in the different applied profiling methods and in the same reprogramming comparisons.

(B) DNA-methylation profiles for probes significantly differing between hESC and iPSC (non-adjusted $p < 0.05$). Colored bars below each cluster indicate cell of origin.

(C) Hierarchically clustered subset of the DNA-methylation probes with the lowest p values (adjusted $p < 0.05$). Associated genes for each probe cluster are indicated on the right.

(D) *PEG3* expression in hESC and iPSC lines. Box and whiskers plot of unique donor PSC values are represented. Anti-correlated gene expression and DNA methylation are denoted by a red alpha. A blue asterisk indicates significant differential expression.

(E) Expression clustering (HOPACH) of genes correlated and anti-correlated with *NANOG* and *MYC* gene expression in all PSC. To the right of this cluster, early- (P0) and late-passage (P10) single-cell hESC (Yan et al., 2013) are shown in the same gene order. Genes with red names are negative regulators of differentiation, stem cell maintenance genes, or positive regulators of cell proliferation, while genes with blue names are associated with ectoderm differentiation, based on ToppGene-associated annotations from multiple sources.

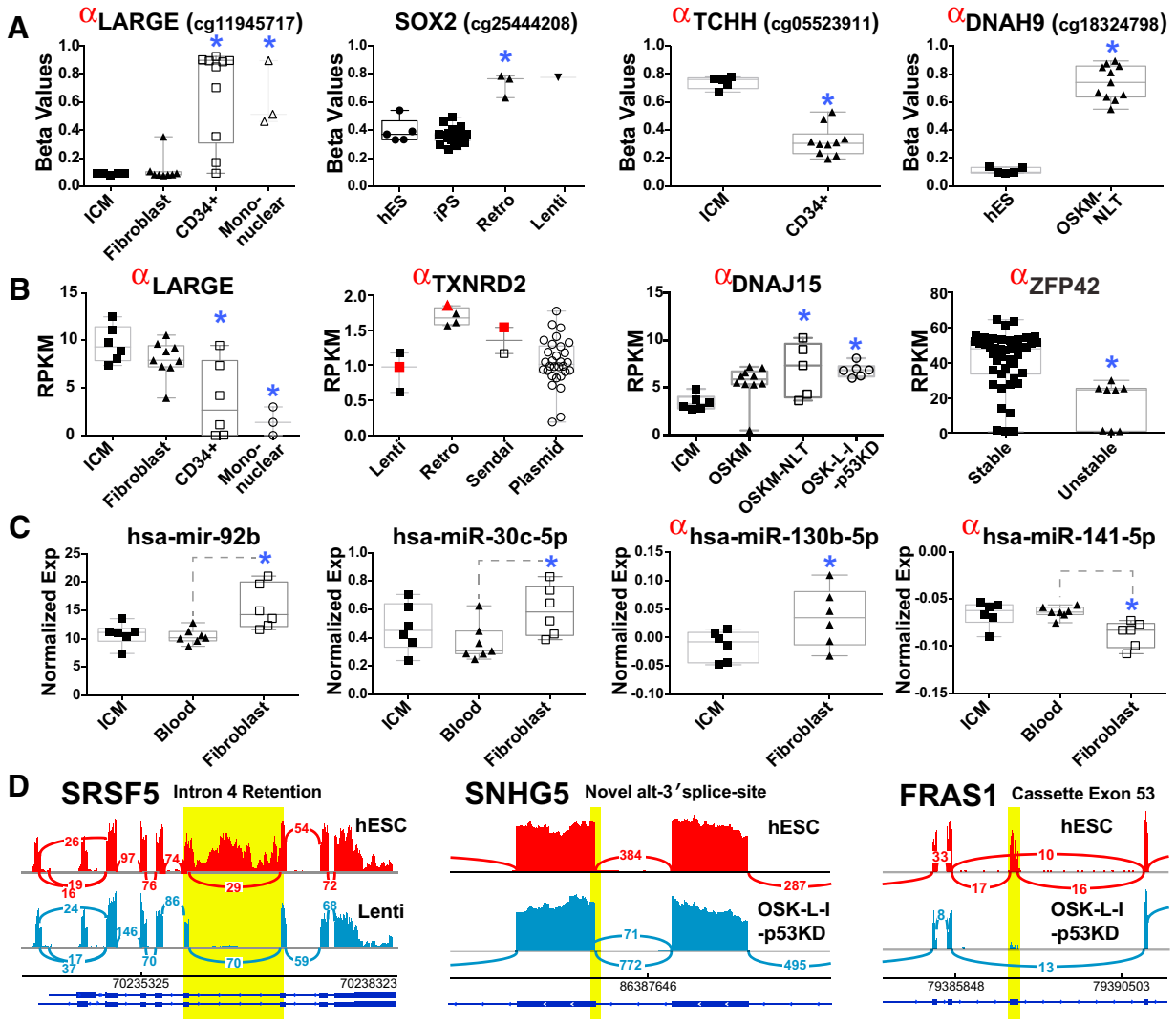

Figure 5. Candidate Factors Associated with iPSC Derivation Method

(A–C) The top differentially regulated (A) DNA methylation, (B) mRNA gene expression, and (C) normalized miRNA expression profiles associated with each indicated comparison. Box and whiskers plot of unique donor PSC values are represented. For TXNRD2, sample expression values for the same genetic donor (D007) are indicated for the three indicated reprogramming methods in red. Anti-correlated gene expression and DNA methylation are denoted by a red alpha. Blue asterisks indicate significantly differentially expressed genes (adjusted $p < 0.05$) versus hESC or the indicated comparator. Retro, retroviral; Lenti, lentiviral; RPKM, reads per kilobase per million mapped reads.

(D) Examples of splicing events visualized in the software IGV (Broad Institute), with associated genomic read-alignment depth and junction read counts indicated for a single representative sample.

retroviral and lentiviral associated genes (e.g., *TXNRD2*, *JUN*, *UCP2*, and *HIST1H2BF*; Figures 5B and S4B) were consistently observed from uniquely reprogrammed lines from a single donor (D007). Notably, these genes are involved in multiple pathways related to oxidative stress. Differential expression of multiple genes affecting cell growth and differentiation (*ID2*, *ID4*, *JAG1*, *IGFBP5*, and *GLT1D1*) were observed with OSK-L-I-p53KD, relative to other gene reprogramming combinations or hESC. In unstable lines, decreased expression of crucial PSC genes (*ZFP42* and *TRIM6*) was associated with increased promoter and gene methylation of these genes. Using a 96-gene qPCR panel we verified differential expression for multiple genes where corresponding probes were present (e.g., *ZFP42*; Figure S4C).

In total, 41 miRNAs were statistically associated with at least one reprogramming variable. Among these, we observed three miRNAs (*miR-92b*, *miR-30c-1*, *miR-30c-2*)

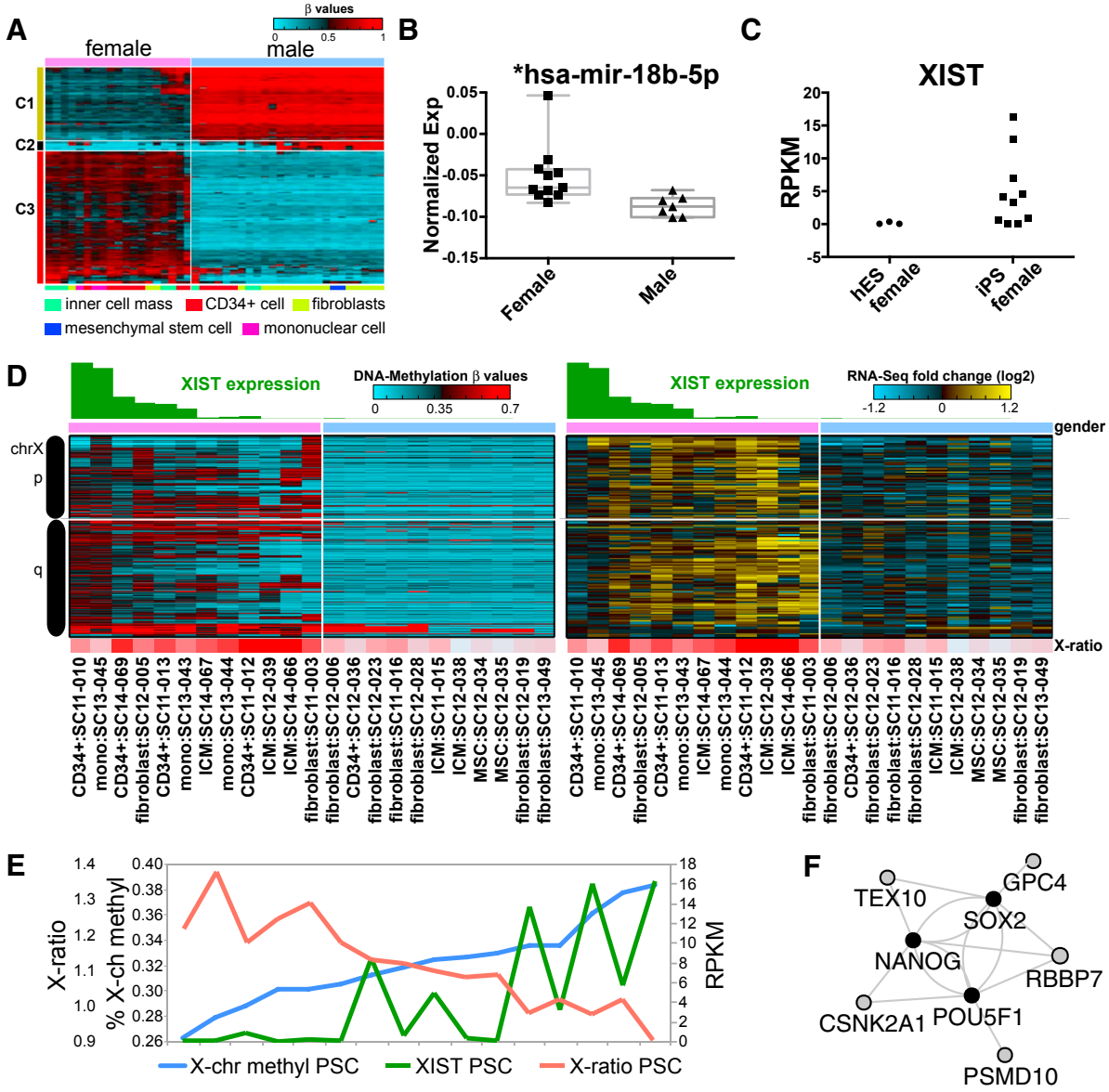

Figure 6. Impact of X-Chromosome Inactivation and Sex on iPSC

(A) Segregation of PSC based on differentially regulated sex-associated DNA-methylated probes (HOPACH).

(B) Normalized miRNA expression values in male and female lines from distinct donors. Box and whiskers plot of unique donor PSC values are represented.

(C) *XIST* expression in independent female hESC and iPSC samples from unique donors.

(D) Heatmaps of all anti-correlated (Pearson $\rho < -0.6$) methylation probes (left) and genes (right) on the X chromosome, ordered by genomic location. *XIST* expression values are in green and X-to-autosome expression ratios are below the heatmaps.

(E) Comparison of distinct measures of XCI within female PSC as determined by RNA-seq (X-to-autosome ratio, *XIST* expression) and DNA-methylation array (% X-chr methylation).

(F) Protein-protein interactions (BioGRID database) between genes anti-correlated with *XIST* (gray) and core pluripotency factors (black).

with predicted mRNA targets that were differentially expressed in a reciprocal manner (GO-Elite) (Figure 5C). Five of the 41 regulated miRNAs were also anti-correlated with methylation probes (*miR-141*, *miR-130b*, *miR-191*, *miR-660*, *miR-548f-1*), suggesting regulation in part by DNA methylation.

Alternative splicing and promoter usage was evaluated in our RNA-seq data. Comparison of hESC and hESC-derived

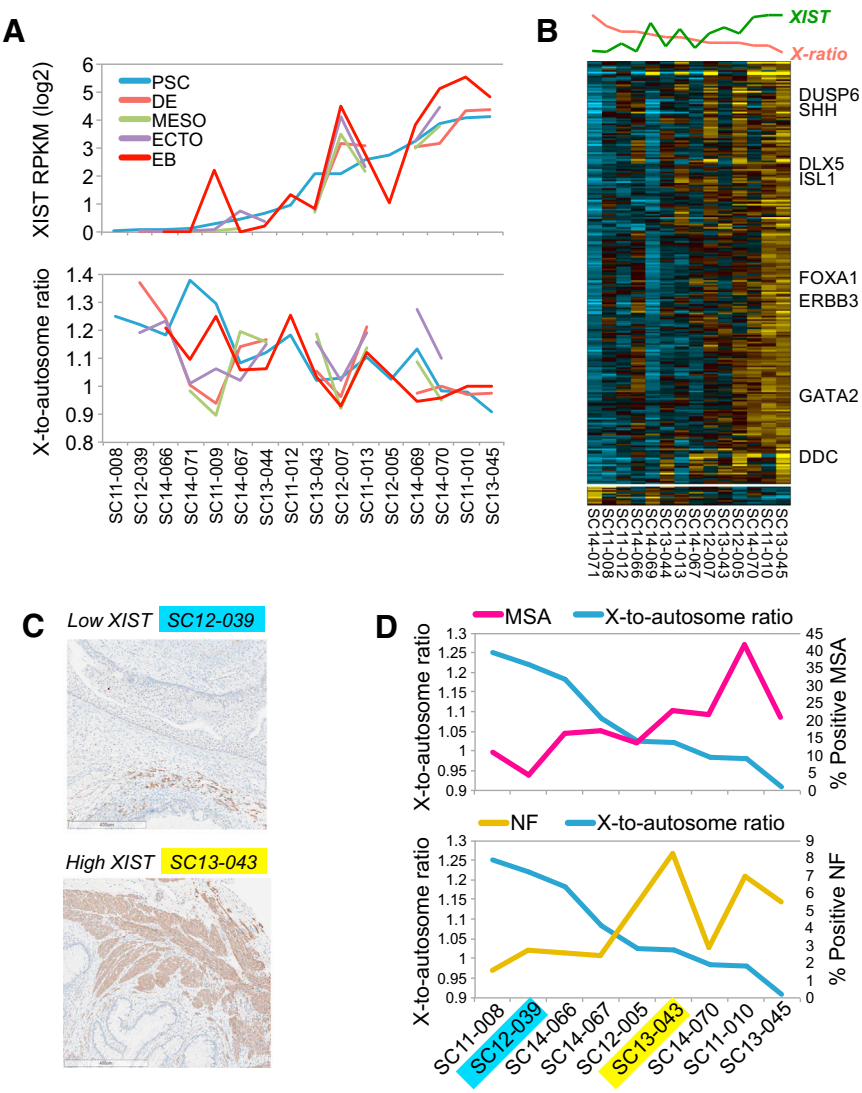

Figure 7. EB Differentiation Outcomes Correlate with Differential X-Chromosome Inactivation among Female Stem Cell Lines

(A) Comparison of *XIST* expression and X-to-autosome ratios in PSC and EB for the same lines (PSC line name indicated below the plots).

(B) HOPACH clustered heatmap of differentially expressed genes in EB differentiated from female PSC lines. Developmental regulators are shown on the right of the plot. PSC X-to-autosome ratio and XIST expression are displayed above the plot.

(C) Immunohistochemistry of two teratomas derived from a low and high XIST female PSC using a muscle-specific actin (MSA) antibody.

(D) Quantification of the percentage of positive MSA or neurofilament (NF) staining in adjacent teratoma sections relative to PSC X-to-autosome ratio.

EBs identified 129 alternative exon events with a false discovery rate $p < 0.05$ (syn3106284), including many well-validated events (in *MBD2*, *DNMT3B*, *SLK*, *ADD3*, *MARK3*, *FYN*, *NUMB*, *NAV2*, and *NFYA*) (Gopalakrishna-Pillai and Iverson, 2011; Lu et al., 2014; Salomonis et al., 2009) (Figure S5A), suggesting that these data are reliable for more in-depth evaluation. A total of 77 alternative exons were significant in a pairwise comparison of all major reprogramming or cell-of-origin variables in PSC. Manual examination of highly differential but non-significant splicing events suggest that many are valid, but detected with lower sensitivity due to reduced sequencing depth (Figures 5D and S5B).

Effect of XCI and Donor Sex

A significant potential confounder in this dataset is donor sex difference. A total of 520 probes were differentially methylated between male and female donors, the majority of which were localized to allosomes (457 probes) (Figure 6A). Similarly, most differentially expressed genes between male and females were also localized to allosomes (43 out of 60), as were differentially expressed miRNA (4 out of 7). Predicted mRNA targets (GO-Elite) of one X-chromosomal miRNA (*miR-18b*) were enriched among male versus female RNA upregulated genes (Figure 6B). This miRNA was also found to be anti-correlated to its own DNA-methylation probes, suggesting that it is regulated by DNA methylation.

Genes associated with autosomal differential DNA methylation were enriched for PRC2 factors and targets of the PRC2 transcription factor *Suz12* (Figures S6B and S6C). Only one DNA-methylation-regulating gene, *MECP2*, was itself differentially methylated between females and males. This is consistent with prior studies

that have identified *MECP2* as a target of X inactivation (Vallot et al., 2015).

In mouse ESC and human somatic cells, aberrant loss of *XIST* expression and corresponding breakdown of normal XCI has been associated with reduced developmental and increased oncogenic potential. In human PSC, *XIST* expression is required for the initiation of XCI but not for XCI maintenance. Multiple classes of female PSC have been described including those which only undergo XCI upon differentiation (class I), those that already have undergone XCI (class II and III), and PSC that have lost *XIST* during culture and have undergone eroded XCI (class III) (Hall et al., 2008; Silva et al., 2008; Vallot et al., 2015). Six of ten iPSC from distinct female donors show little to no *XIST* expression by RNA-seq, with no expression in any of the three hESC (Figure 6C). Restricted analysis of probes on the X chromosome found 1,118 methylation probes anti-correlated for the same PSC with gene expression (syn3107536). These largely overlapped with a prior set of described XCI-associated probes, 619 out of 3,279 (Nazor et al., 2012) (syn3107535). From these 1,118 probes, we find that lines without *XIST* expression have a decrease in X-chromosome methylation and increased X-to-autosome gene-expression ratio (Figures 6D and S6C). Each of these three measures of XCI were correlated to each other ($\rho > 0.6$ or $\rho < -0.6$) (Figure 6E). The observed continuum of predicted XCI among PSC lines supports prior proposed models of variable or precocious XCI among cells within each PSC line, rather than 100% conformity (Hall et al., 2008; Silva et al., 2008). Although spontaneous differentiation in some cultures could account for the increased XCI, both *XIST* expression and X-to-autosome ratios were largely consistent in biological RNA-seq replicates from the same PSC line (data not shown). Among 116 genes anti-correlated (Pearson $\rho < -0.6$) with *XIST* expression, five (*RBBP7*, *CSNK2A1*, *PSMD10*, *GPC4*, and *TEX10*) shared protein interactions with at least one core pluripotency factor (*POU5F1*, *SOX2*, or *NANOG*) (BioGRID database). The X-chromosome localized nucleosome remodeling factor *RBBP7* was the most anti-correlated with *XIST* expression and interacts with all three pluripotency factors at the protein level (Figure 6E).

In addition to these expression differences, 646 autosome and allosome probes were differentially methylated in XIST-high versus XIST-low female lines (unique donors, all probes considered). Among the 236 known associated genes, eight transcription factors were hypermethylated (*Brachyury*, *ZNF628*, *CUX1*) or hypomethylated (*MZF1*, *SCRT2*, *SCML1*, *TFCP2*, *ZNF148*) with high *XIST* expression. Several of these factors have important roles in lineage differentiation (*Brachyury*, *SCRT2*, *TFCP2*, *CUX1*) or proliferation (*MZF1*, *ZNF148*, *CUX1*) (Figure S6D). As these genes promote distinct differentiation pathways, we subjected a set of female PSC (n = 16) to short-term directed differentiation assays for definitive endoderm, mesoderm, ectoderm, and EB and performed RNA-seq. Although *XIST* expression in these lines changed upon differentiation, high *XIST* lines generally remained high (average 2-fold increase versus PSC) and *XIST*-low remained low (Figure 7A). While most of these lines retained similar X-to-autosome ratios during differentiation as well, notable variance among a few lines was observed (SC11-009, SC14-069, SC14-071) (Figure 7A). Comparison of the number of passages in these two sets of lines revealed that low *XIST* PSC had undergone significantly more passages in culture (Student's t test $p < 0.05$, ~6 passages more on average). At least one prior study has demonstrated that failure to induce to *XIST* expression upon PSC differentiation is a hallmark of XCI erosion (Mekhoubad et al., 2012). Taken together, the low *XIST* female PSC in this study appear to be most consistent with class III or eroded XCI. An exception to this rule was SC11-009. This line was found to transition from low to high *XIST* expression from the PSC to the EB. This same trend was observed in all lineage and EB differentiations, suggesting induction of XCI (class I).

To analyze the differentiation gene-expression results in the context of XCI, we focused on genes with expression correlated ($\rho > 0.6$ or $\rho < -0.6$) to multiple measures of PSC XCI in each differentiation state (PSC *XIST* expression, X-to-autosome ratio, and degree of X-chromosome methylation). In EB, we found 267 genes correlated to multiple measures of XCI and only 12 anti-correlated (Figure 7B). These correlated genes were most enriched (ToppGene) in proteins associated with methylation (e.g., *TRMT11*, *COMTD1*, *HENMT1*, *CAMKMT*), neuron-fate commitment (*GATA2 ISL1*, *FOXA1*, *SHH*), heart development (*ERBB3*, *ISL1*, *SSH*), and other broad developmental processes. Analysis of the early germ-layer differentiations revealed possible precocious induction of genes anti-correlated with measures of XCI in each of the differentiations, such as *myocardin* and *SMAD3* in definitive endoderm (Figure S6E, syn5565603). As an improved means to evaluate the differentiation potential of these lines, we performed immunohistochemistry on teratoma sections from female PSC (Figures 7C, 7D, and S6F). On average, we detected ~18% positive MSA staining and ~4% neurofilament (NF) staining in adjacent histological sections. Strikingly, both differentiation markers were correlated to multiple measures of PSC XCI (>0.6), with MSA most highly correlated to *XIST* expression ($\rho = 0.71$) and NF to X-to-autosome ratio ($\rho = 0.67$). These results are in agreement with prior studies indicating that PSC with increased *XIST* and XCI results in improved

differentiations relative to PSC undergoing XCI erosion (Mekhoubad et al., 2012).

DISCUSSION

The large-scale profiling of dozens of iPSC and previously characterized hESC represents an important analytical reference for the stem cell research community. Evaluating these lines using the same post-reprogramming culture conditions and profiling technologies has allowed us to carefully examine many possible variables. The creation of metadata standards and associated ontologies was essential to make informed comparisons and identify confounders in our study. All metadata, raw genomic files, protocols, processed results, and analyses are provided in Synapse (Omberg et al., 2013).

Our studies identified 23 iPSC lines with adverse characteristics such as contamination, karyotypic abnormalities, flow cytometry, or culture morphology consistent with differentiation. Surprisingly, teratomas generated from 45 of 46 lines, including three with characteristics of differentiation, were pluripotent as they contained cells from all three embryonic germ layers. Notably, three pluripotent teratomas also contained undifferentiated cells identified by histological or immunostaining analyses, although independent tumors from the same lines were fully differentiated and did not. Given that the teratoma assay is commonly used to confirm PSC pluripotency and quality (Muller et al., 2010), these results suggest that teratoma analysis should be considered within the context of other analyses and results to determine the quality of the PSC line and not as a stand-alone quality measure.

Evaluation of deleterious CNV provided strong evidence that the same genetic abnormalities can occur in distinct iPSC lines and that such abnormalities can arise during the reprogramming process. As described in other studies, we were unable to exclude the possibility that there was heterogeneity in the starting cell population (Ma et al., 2014). CNV that were coincident with differential expression frequently resulted in the deletion of known tumor suppressors or duplication of cell growth/oncogenic factors. Such genetic abnormalities could result in clonal selection advantages that are undesirable for clinical applications (Cunningham et al., 2012).

The DNA-methylation, gene-expression, miRNA, and splicing differences observed in these studies represent intriguing differences in PSC that could result in differences in pluripotentiality, cell growth, or potential tumorigenicity in vivo. The existence of consistent patterns between DNA methylation and mRNA or miRNA expression provides an additional layer of confidence in these observations. While methylation profiles were highly and consistently different among iPSC and hESC, fewer differences were observed for mRNA and miRNA. Although many DNA-methylation probes were identified that were highly distinct between iPSC and hESC, including a number of probes anti-correlated with gene expression (*FRG1B*, *CCL28*, *CR1L*, *PEG3*), none could perfectly distinguish between these cell types.

At a global level, the analysis of DNA-methylation profiles provides important insights into molecular and cell growth characteristics of PSC that would otherwise be difficult to identify. Reprogramming-associated variations in X-linked CpG methylation is of particular interest because of the complex variations in degrees of XCI and X-chromosome reactivation between various hierarchical states of pluripotency. Our analysis highlighted two distinct populations of XCI female cells, with the most hypermethylated X-chromosomal PSC split between very high and absent *XIST* expression. Interestingly, none of the female hESC lines in this study expressed *XIST*, whereas many of the iPSC do. Our analyses of differentiated female PSC identified correlates between XCI and pluripotentiality that substantiate prior proposed models and provide additional candidate molecular regulators for investigation (Mekhoubad et al., 2012; Silva et al., 2008).

Genes anti-correlated with *XIST*, principally *RBBP7*, share protein interactions with core pluripotency regulators, and these differences persist in the EB. This result is particularly intriguing given that *RBBP7*, a partner of PRC2 implicated in nucleosome binding, and *SUZ12*, a component of PRC2 required for stability of the complex and EZH1/2 mediated catalytic activity, were highly enriched factors in our analysis of differentially methylated sex-associated autosomal genes. In addition to *RBBP7*, predicted regulation by PRC2 was recurrent in a number of our covariate analyses, including iPSC versus hESC differentially methylated probes. A growing body of literature now supports an important role for PRC2 in pluripotency, XCI, and differentiation as a recruitment tool of PRC1 (Cheng et al., 2014). Although likely not relevant in vivo, such physical protein and epigenetic interactions could be undesirable in iPSC for programmed lineage differentiation.

The resource presented here provides a standardized and annotated dataset for the characterization of hESC and iPSC that can be applied to the discovery of molecular determinants underlying specific biological properties of iPSC and their use for future clinical applications. It provides information on the most relevant, informative, and efficient assays to use for iPSC characterization. Finally, the new data repository encodes a standard for the biological, genomic, and epigenomic characteristics of high-quality, stable iPSC that will serve as a valuable resource as iPSC technology moves into clinical translation. The

many observed reprogramming and cell-of-origin gene-expression and splicing differences provide intriguing starting hypotheses to fuel new research.

We aim to improve the breadth and utility of this new resource by adding additional pluripotent lines and differentiated products. Integration of previously published and new datasets will further facilitate advanced cross-comparison analyses, many of which can be achieved using the online data analysis and exploratory tools provided within the Synapse programmatic and web interface. By providing consistent cell-line descriptions, protocols, and associated data in an easy-to-access online repository, we hope that these observations will fuel future research into the role of these gene signatures in resulting progenitor populations.

EXPERIMENTAL PROCEDURES

Methods and Data Availability

All data and methods described herein are available at https://www.synapse.org/PCBC (http://dx.doi.org/10.7303/syn1773109) and/or Supplemental Experimental Procedures. Accessions for specific methods are provided in methods sections and Table S9. For interactive analyses, customized data exploration options have been integrated into Synapse to facilitate gene-level, cluster, and ToppGene functional enrichment analyses.

Cell Lines

The lines brought into the study included commonly used but distinct variables from multiple laboratories (Figure 2A). The line identifiers, originating laboratory, and key contributing scientists for each line are provided in Table S1.

Genomic and Epigenetic Molecular Characterization

mRNA-Seq libraries were prepared with the Illumina TruSeq kit RNA V2. Single-end libraries were sequenced at a depth of between 10 and 30 million 50-nt reads on an Illumina HiSeq 2000. A small number (n = 3) of ESC and iPSC were also sequenced at a depth of ~50 million paired-end, stranded reads, for comparison. miRNA libraries were prepared with the Illumina TruSeq Small RNA kit and sequenced to 1–4 million reads. Methylation was assessed with the Illumina HumanMethylation450 BeadChip with annotations provided by ENCODE (Encode Project Consortium, 2012). Two different assays were used for CNV analysis. 21 cell lines were assayed with the Illumina CytoSNP-850K BeadChip, and 29 cell lines with the Illumina HD HumanOMNI-Quad BeadChip platform. Thirty-seven lines were assayed using a TaqMan Low Density Array (Life Technologies, 4385344) containing a panel of stem cell and pluripotency marker genes (syn3107327).

Data Processing

FASTQ files were aligned to the human genome build GRCh37 and University of California Santa Cruz transcriptome reference (Rosenbloom et al., 2014) using TopHat 2.0.9 (Kim et al., 2013) (syn1773110). Gene-level RPKM (reads per kilobase per million mapped reads) and alternative splicing estimates were obtained from AltAnalyze (Emig et al., 2010). miRNA expression was quantified with mirExpress v2.1.4 (Wang et al., 2009) using the human miRBase 20.0 reference (syn2247097). Methylation arrays were normalized with the minfi R package (Aryee et al., 2014) (syn2677441). Raw data and processing scripts with exact parameters used are available and are linked together by provenance in Synapse (Table S9).

SUPPLEMENTAL INFORMATION

Supplemental Information includes Supplemental Experimental Procedures, Supplemental Results, six figures, and nine tables and can be found with this article online at http://dx.doi.org/10.1016/j.stemcr.2016.05.006.

AUTHOR CONTRIBUTIONS

J.W., W.H., A.K.H., P.M., A.M., J.A.C., B.A., and C.L. conceived of and designed the study. N.S., P.J.D., L.O., R.S., S.B., L.S., S.H.S., M.K., C.M., K.D., and S.H. generated and assembled the data. N.S., P.J.D., L.O., R.S., S.B., J.H., M.K., S.K.S., K.D., Y.W., E.Z., P.M., J.A.C., B.A., and C.L. analyzed and interpreted the data. N.S., P.J.D., L.O., L.S., S.H.S., J.H., and C.L. wrote the manuscript.

ACKNOWLEDGMENTS

The authors thank the PCBC line contributors in Table S1; Dr. Michael Terrin, Ling Tang, Andrea Lefever, and Liz Casher from the Administrative Coordinating Center; and Dr. Elke Grassman and Diana Nordling from the CCHMC Translational Core Laboratories for support. This work was supported by the NHLBI Progenitor Cell Biology Consortium, Administrative Coordinating Center (U01HL099997), Cell Characterization Core, Bioinformatics Core, and PCBC2012Pilot_01. Other support was provided by the National Heart, Lung, and Blood Institute (NHLBI) (U01HL099775), the National Institute for Child Health and Human Development (NICHD) (R01HD082098), the National Institute General Medical Sciences (NIGMS) (R01GM110628), and the National Eye Institute (NEI) (R01EY023962). Under a licensing agreement between Life Technologies Corporation and the Johns Hopkins University, E.Z. is entitled to a share of royalty received by the University on sales of human induced pluripotent stem cell lines. The terms of this arrangement are being managed by the Johns Hopkins University in accordance with its Conflict of Interest policies.

Received: August 31, 2015
Revised: May 9, 2016
Accepted: May 10, 2016
Published: June 9, 2016

REFERENCES

Abyzov, A., Mariani, J., Palejev, D., Zhang, Y., Haney, M.S., Tomasini, L., Ferrandino, A.F., Rosenberg Belmaker, L.A., Szekely, A., Wilson, M., et al. (2012). Somatic copy number mosaicism in human skin revealed by induced pluripotent stem cells. Nature *492*, 438–442.

Aryee, M.J., Jaffe, A.E., Corrada-Bravo, H., Ladd-Acosta, C., Feinberg, A.P., Hansen, K.D., and Irizarry, R.A. (2014). Minfi: a flexible

and comprehensive Bioconductor package for the analysis of Infinium DNA methylation microarrays. Bioinformatics *30*, 1363–1369.

Bock, C., Kiskinis, E., Verstappen, G., Gu, H., Boulting, G., Smith, Z.D., Ziller, M., Croft, G.F., Amoroso, M.W., Oakley, D.H., et al. (2011). Reference maps of human ES and iPS cell variation enable high-throughput characterization of pluripotent cell lines. Cell *144*, 439–452.

Chen, J., Bardes, E.E., Aronow, B.J., and Jegga, A.G. (2009). ToppGene Suite for gene list enrichment analysis and candidate gene prioritization. Nucleic Acids Res. *37*, W305–W311.

Cheng, B., Ren, X., and Kerppola, T.K. (2014). KAP1 represses differentiation-inducible genes in embryonic stem cells through cooperative binding with PRC1 and derepresses pluripotency-associated genes. Mol. Cell. Biol. *34*, 2075–2091.

Clancy, J.L., Patel, H.R., Hussein, S.M., Tonge, P.D., Cloonan, N., Corso, A.J., Li, M., Lee, D.S., Shin, J.Y., Wong, J.J., et al. (2014). Small RNA changes en route to distinct cellular states of induced pluripotency. Nat. Commun. *5*, 5522.

Cunningham, J.J., Ulbright, T.M., Pera, M.F., and Looijenga, L.H. (2012). Lessons from human teratomas to guide development of safe stem cell therapies. Nat. Biotechnol. *30*, 849–857.

Emig, D., Salomonis, N., Baumbach, J., Lengauer, T., Conklin, B.R., and Albrecht, M. (2010). AltAnalyze and DomainGraph: analyzing and visualizing exon expression data. Nucleic Acids Res. *38*, W755–W762.

Encode Project Consortium (2012). An integrated encyclopedia of DNA elements in the human genome. Nature *489*, 57–74.

Gopalakrishna-Pillai, S., and Iverson, L.E. (2011). A DNMT3B alternatively spliced exon and encoded peptide are novel biomarkers of human pluripotent stem cells. PLoS One *6*, e20663.

Hall, L.L., Byron, M., Butler, J., Becker, K.A., Nelson, A., Amit, M., Itskovitz-Eldor, J., Stein, J., Stein, G., Ware, C., et al. (2008). X-inactivation reveals epigenetic anomalies in most hESC but identifies sublines that initiate as expected. J. Cell. Physiol. *216*, 445–452.

International Stem Cell Initiative, Adewumi, O., Aflatoonian, B., Ahrlund-Richter, L., Amit, M., Andrews, P.W., Beighton, G., Bello, P.A., Benvenisty, N., Berry, L.S., et al. (2007). Characterization of human embryonic stem cell lines by the International Stem Cell Initiative. Nat. Biotechnol. *25*, 803–816.

Kim, D., Pertea, G., Trapnell, C., Pimentel, H., Kelley, R., and Salzberg, S.L. (2013). TopHat2: accurate alignment of transcriptomes in the presence of insertions, deletions and gene fusions. Genome Biol. *14*, R36.

Lee, D.S., Shin, J.Y., Tonge, P.D., Puri, M.C., Lee, S., Park, H., Lee, W.C., Hussein, S.M., Bleazard, T., Yun, J.Y., et al. (2014). An epigenomic roadmap to induced pluripotency reveals DNA methylation as a reprogramming modulator. Nat. Commun. *5*, 5619.

Lu, Y., Loh, Y.H., Li, H., Cesana, M., Ficarro, S.B., Parikh, J.R., Salomonis, N., Toh, C.X., Andreadis, S.T., Luckey, C.J., et al. (2014). Alternative splicing of MBD2 supports self-renewal in human pluripotent stem cells. Cell Stem Cell *15*, 92–101.

Ma, H., Morey, R., O'Neil, R.C., He, Y., Daughtry, B., Schultz, M.D., Hariharan, M., Nery, J.R., Castanon, R., Sabatini, K., et al. (2014). Abnormalities in human pluripotent cells due to reprogramming mechanisms. Nature *511*, 177–183.

McConnell, M.J., Lindberg, M.R., Brennand, K.J., Piper, J.C., Voet, T., Cowing-Zitron, C., Shumilina, S., Lasken, R.S., Vermeesch, J.R., Hall, I.M., et al. (2013). Mosaic copy number variation in human neurons. Science *342*, 632–637.

Mekhoubad, S., Bock, C., de Boer, A.S., Kiskinis, E., Meissner, A., and Eggan, K. (2012). Erosion of dosage compensation impacts human iPSC disease modeling. Cell Stem Cell *10*, 595–609.

Muller, F.J., Goldmann, J., Loser, P., and Loring, J.F. (2010). A call to standardize teratoma assays used to define human pluripotent cell lines. Cell Stem Cell *6*, 412–414.

Müller, F.J., Schuldt, B.M., Williams, R., Mason, D., Altun, G., Papapetrou, E.P., Danner, S., Goldmann, J.E., Herbst, A., Schmidt, N.O., et al. (2011). A bioinformatic assay for pluripotency in human cells. Nat. Methods *8*, 315–317.

Nazor, K.L., Altun, G., Lynch, C., Tran, H., Harness, J.V., Slavin, I., Garitaonandia, I., Muller, F.J., Wang, Y.C., Boscolo, F.S., et al. (2012). Recurrent variations in DNA methylation in human pluripotent stem cells and their differentiated derivatives. Cell Stem Cell *10*, 620–634.

Nguyen, H.T., Geens, M., Mertzanidou, A., Jacobs, K., Heirman, C., Breckpot, K., and Spits, C. (2014). Gain of 20q11.21 in human embryonic stem cells improves cell survival by increased expression of Bcl-xL. Mol. Hum. Reprod. *20*, 168–177.

Omberg, L., Ellrott, K., Yuan, Y., Kandoth, C., Wong, C., Kellen, M.R., Friend, S.H., Stuart, J., Liang, H., and Margolin, A.A. (2013). Enabling transparent and collaborative computational analysis of 12 tumor types within the Cancer Genome Atlas. Nat. Genet. *45*, 1121–1126.

Osborne, M.J., Volpon, L., Kornblatt, J.A., Culjkovic-Kraljacic, B., Baguet, A., and Borden, K.L. (2013). eIF4E3 acts as a tumor suppressor by utilizing an atypical mode of methyl-7-guanosine cap recognition. Proc. Natl. Acad. Sci. USA *110*, 3877–3882.

Rosenbloom, K.R., Armstrong, J., Barber, G.P., Casper, J., Clawson, H., Diekhans, M., Dreszer, T.R., Fujita, P.A., Guruvadoo, L., Haeussler, M., et al. (2014). The UCSC Genome Browser database: 2015 update. Nucleic Acids Res. *43*, D670–D681.

Rouhani, F., Kumasaka, N., de Brito, M.C., Bradley, A., Vallier, L., and Gaffney, D. (2014). Genetic background drives transcriptional variation in human induced pluripotent stem cells. PLoS Genet. *10*, e1004432.

Salomonis, N., Nelson, B., Vranizan, K., Pico, A.R., Hanspers, K., Kuchinsky, A., Ta, L., Mercola, M., and Conklin, B.R. (2009). Alternative splicing in the differentiation of human embryonic stem cells into cardiac precursors. PLoS Comput. Biol. *5*, e1000553.

Schlaeger, T.M., Daheron, L., Brickler, T.R., Entwisle, S., Chan, K., Cianci, A., DeVine, A., Ettenger, A., Fitzgerald, K., Godfrey, M., et al. (2015). A comparison of non-integrating reprogramming methods. Nat. Biotechnol. *33*, 58–63.

Silva, S.S., Rowntree, R.K., Mekhoubad, S., and Lee, J.T. (2008). X-chromosome inactivation and epigenetic fluidity in human embryonic stem cells. Proc. Natl. Acad. Sci. USA *105*, 4820–4825.

Takahashi, K., and Yamanaka, S. (2006). Induction of pluripotent stem cells from mouse embryonic and adult fibroblast cultures by defined factors. Cell *126*, 663–676.

Thomson, J.A., Itskovitz-Eldor, J., Shapiro, S.S., Waknitz, M.A., Swiergiel, J.J., Marshall, V.S., and Jones, J.M. (1998). Embryonic stem cell lines derived from human blastocysts. Science *282*, 1145–1147.

Tonge, P.D., Corso, A.J., Monetti, C., Hussein, S.M., Puri, M.C., Michael, I.P., Li, M., Lee, D.S., Mar, J.C., Cloonan, N., et al. (2014). Divergent reprogramming routes lead to alternative stem-cell states. Nature *516*, 192–197.

Vallot, C., Ouimette, J.F., Makhlouf, M., Feraud, O., Pontis, J., Come, J., Martinat, C., Bennaceur-Griscelli, A., Lalande, M., and Rougeulle, C. (2015). Erosion of X chromosome inactivation in human pluripotent cells initiates with XACT coating and depends on a specific heterochromatin landscape. Cell Stem Cell *16*, 533–546.

Wang, W.C., Lin, F.M., Chang, W.C., Lin, K.Y., Huang, H.D., and Lin, N.S. (2009). miRExpress: analyzing high-throughput sequencing data for profiling microRNA expression. BMC Bioinformatics *10*, 328.

Yan, L., Yang, M., Guo, H., Yang, L., Wu, J., Li, R., Liu, P., Lian, Y., Zheng, X., Yan, J., et al. (2013). Single-cell RNA-seq profiling of human preimplantation embryos and embryonic stem cells. Nat. Struct. Mol. Biol. *20*, 1131–1139.

Young, M.A., Larson, D.E., Sun, C.W., George, D.R., Ding, L., Miller, C.A., Lin, L., Pawlik, K.M., Chen, K., Fan, X., et al. (2012). Background mutations in parental cells account for most of the genetic heterogeneity of induced pluripotent stem cells. Cell Stem Cell *10*, 570–582.

Stem Cell Reports, Volume *7*

Supplemental Information

Integrated Genomic Analysis of Diverse Induced Pluripotent Stem Cells from the Progenitor Cell Biology Consortium

Nathan Salomonis, Phillip J. Dexheimer, Larsson Omberg, Robin Schroll, Stacy Bush, Jeffrey Huo, Lynn Schriml, Shannan Ho Sui, Mehdi Keddache, Christopher Mayhew, Shiva Kumar Shanmukhappa, James Wells, Kenneth Daily, Shane Hubler, Yuliang Wang, Elias Zambidis, Adam Margolin, Winston Hide, Antonis K. Hatzopoulos, Punam Malik, Jose A. Cancelas, Bruce J. Aronow, and Carolyn Lutzko

Supplemental Information

Study Design

The PCBC Core Standards Working Group identified the characteristics for the iPSC included in the study based on donor cell type, reprogramming vector and gene combinations. The Cincinnati Cell Characterization Core (C4) established standard protocols for thaw, adaptation to standardized feeder-free culture conditions, sample collection and analysis. Manufacturer lots were tested and controlled for standardization of key reagents. Lines were thawed directly into feeder-free mTeSR1 culture media on Matrigel (hereafter referred to as feeder-free) regardless of the conditions under which they were cultured or cryopreserved in the originating laboratory (syn2724705). Cell lines that did not viably recover using this strategy were subsequently re-thawed onto irradiated murine embryonic feeders (MEFs) with hES media using standard conditions (Thomson et al., 1998) or were re-requested to be sent as live cultures on MEFs from the originating laboratory. In either of these cases the cells were subsequently transitioned into the feeder-free conditions prior to downstream analysis.

Standardizing Metadata Fields, Terms, Collection and Confirmation

Metadata information was initially provided by the originating laboratory, and was subsequently augmented with *in vitro* genetic and experimental characterization data of the line, and resubmitted to the originating lab for confirmation. For example, sex was confirmed with karyotype results and lines submitted by a common donor were identified from SNP calls derived from genotyping arrays and RNA-Seq. Specifically an identity-by-descent analysis was performed in PLINK (Purcell et al., 2007) first using the subset of individuals for which genotyping had been performed and then verified with SNP calls based on RNA-Seq from a larger subset of samples which identified three more samples with common donors. The source SNP array PLINK input files and merged VCF genotype file are available (syn2391784).

iPSC Cell Culture, Flow Cytometry and Molecular Sample Collection

iPSC were cultured in mTeSR1 (Stem Cell Technologies, Vancouver, Canada) on Matrigel (Corning Inc., Corning, New York) coated 6-well dishes (Nunc, Waltham,

Massachusetts) and subcultured with dispase using protocols adapted from the manufacturer (syn2724700).

For analysis of cell surface markers, cells were harvested with Accutase (Innovative Cell Technologies, San Diego, California), blocked with 2% IVIG and 1% HSA in PBS, and stained with the specific antibodies for 30 minutes at +4°C. For intracellular marker analysis, cells were fixed and permeabilized with the Becton Dickinson Fix/Perm Kit (BD Biosciences, San Jose, California) prior to addition of antibodies. Samples were subjected to flow cytometry acquisition on a MACSQuant cytometer (Miltenyi Biotech, San Diego, California) and analyzed using FlowJo software (FlowJo, Ashland, Oregon).

Samples for mRNA and miRNA analysis were prepared by removing culture media from and adding 1mL Trizol Reagent (Ambion, Carlsbad, California) per well and incubating for 1 minute. Trizol was pipetted several times, transferred to RNAse-free tubes, and stored at -80°C until extraction. Samples were extracted using manufacturer's recommended protocols using chloroform:isoamyl alcohol (49:1) followed by ethanol precipitation and split into 2 aliquots. Half the sample was pelleted and retained for miRNA-Seq analysis without further preparation. The other half was subjected to mRNA purification using PureLink Spin Cartridges (Life Technologies, Carlsbad, California). Samples for DNA analysis were prepared by removing culture media from the plate, scraping the cell layer with a cell scraper, and collecting in DPBS. The cell suspension was centrifuged for 1 minute at 1000xg and excess DPBS was removed from the pellet. The pellet was stored at -80°C until DNA was isolated.

In vitro and In vivo Pluripotency Analysis

Cells were harvested for RNA, DNA, and flow cytometry as described above. Detailed protocols are available in the Synapse database (syn2512369). Cells were additionally differentiated in embryoid body (EB) cultures for 17 days. In brief, iPSC were disaggregated into clumps and cultured in suspension on non-adherent culture dishes. On day 7, the EB were transferred to gelatin coated tissue culture dishes where they adhered, and grew out from the EB On day 17, the cultures were harvested for DNA and RNA extraction and analysis (syn2512370).

Each line was also subjected to an *in vivo* teratoma pluripotency assay. In brief, 80-90% confluent plates were incubated in dispase for 2-3 minutes, washed with DMEM/F-12 media, and scraped to retain small clumps. The clumps were pelleted and

resupended in 30% Matrigel in mTeSR1 for injection into NOD.Cg-*Prkdc*^{scid}*Il2rg*^{tm1Wjl}/SzJ mice (NSG mice) from the Cincinnati Children's Hospital Medical Center (CCHMC) Comprehensive Mouse and Cancer Core. Tumors were harvested when they reached ~1cm^3 and were fixed in 4% paraformaldehyde. Tumors were paraffin embedded, sectioned, stained in hematoxylin-eosin and evaluated in the clinical pathology core at CCHMC using standard procedures (syn3103753).

Stained histological sections (syn2882776) and a table with the pathologist observations and interpretations of sections from every line are available (syn2882785) with an example in Figure S1.

Molecular Karyotypic Copy Number Variation Analysis of iPSC

CNV were classified as benign, non-benign or clinically significant by Board Certified Clinical Cytogeneticists using the Cincinnati Children's Hospital clinical genetics database. To determine differential gene expression compared to observed non-benign CNV occurrence, at least a 50% change in expression from the mean of all PSC was required. As two distinct Illumina genotyping arrays were used for these studies (syn1773109), for all described comparisons between PSC derived from the same donor, we required that the results were obtained from a single genotyping array platform.

Data Exploration and Distribution

To provide comprehensive data and evaluations of each line, all associated data has been deposited into the Synapse online data repository (syn1773109). This includes metadata, *in vitro* and *in vivo* differentiation, qPCR, RNA- and miRNA-seq, CNV and DNA methylation high-throughput sequence and processed data. In addition to data files, associated analysis code, analytical methods and provenance tracking for all associated files have been included. To aid in interactive analyses of this data, customized data exploration options have been integrated into Synapse to facilitate gene-level analysis, cluster analysis and ToppGene functional enrichment analysis.

Genomic and Epigenetic Molecular Characterization

Details on the protocols and technologies employed are included in the supplementary

file, along with raw and processed data files in Synapse (syn1773109). To assay gene expression levels, total RNA was extracted and prepared with the Illumina TruSeq kit RNA V2. Single-end libraries were sequenced at a depth of between 10-30 million 50nt reads on an Illumina HiSeq 2000. miRNA expression levels were evaluated in a similar fashion, except that libraries were prepared with the Illumina TruSeq Small RNA kit and sequenced to only 1-4 million reads. Methylation was assessed with the Illumina HumanMethylation450 BeadChip with annotations provided by ENCODE (Encode Project Consortium, 2012). Two different assays were used for copy number variation (CNV) analysis: 21 cell lines were assayed with the Illumina CytoSNP-850K BeadChip, and 29 cell lines were assayed with the Illumina HD HumanOMNI-Quad BeadChip platform. For validation, 37 lines were analyzed using a TaqMan Low Density Array (TLDA) (Stem Cell Pluripotency Array, 4385344, Life Technologies) that evaluates a panel of stem cell and pluripotency marker genes (syn3107327).

Sensitivity Assessment of the PSC RNA-Seq

Prior to performing RNA-Seq on all PSC samples, we compared the use of deep (~50 million) sequenced paired-end (PE), stranded RNA-Seq (50nt reads) to that of more-shallow (~20 million) single-end (SE), non-stranded reads. Comparison of SE and PE for the same iPSC (n=2) and ESC (n=1), yielded an r^2 value of greater than 0.96 for all comparisons. For all of these comparisons, the number of PE gene measurements RPKM>1, was equivalent to the SE, lower depth samples, suggesting that these parameters are sufficiently to accurately quantify gene expression.

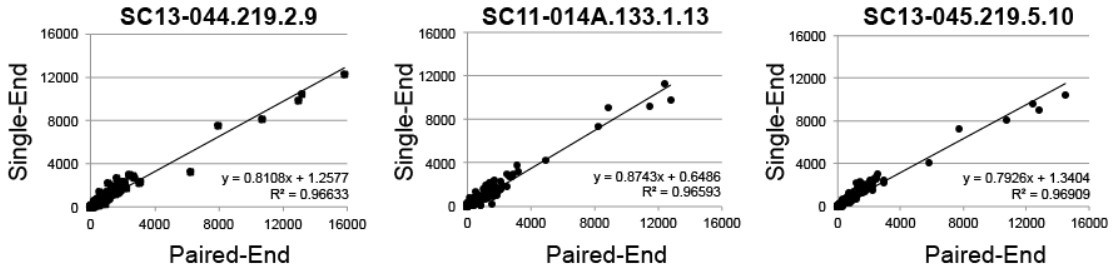

Sample ID	Sequencing Parameter	PSC	Number of Genes RPKM>1
SC13-045_PE.463.1.708	PE	iPSC	13,875
SC13-045.219.5.10	SE	iPSC	14,241
SC11-014_PE.457.1.703	PE	ESC	13,956
SC11-014A.133.1.13	SE	ESC	14,554
SC13-044_PE.457.1.705	PE	iPSC	13,774

SC13-044.219.2.9	SE	iPSC	14,213

RNA-Seq Data Processing

FASTQ files were aligned to the human genome build GRCh37 and University of California Santa Cruz (UCSC) transcriptome reference (Rosenbloom et al., 2014) using Tophat 2.0.9 (Kim et al., 2013). Processing scripts with exact parameters used and raw data are available and are linked together by provenance in Synapse (syn1773110). Gene-level Reads Per Kilobase per Million (RPKM) values and alternative splicing estimates were obtained using AltAnalyze (Emig et al., 2010). All samples were evaluated for a variety of quality control metrics including alignment percentage, proportion of exonic reads, and distribution of reads at the 5' and 3' ends of transcripts using the Cincinnati Children's Medical Center DNA sequencing core automated pipeline. Outlier samples with poor 5' to 3' ratios or other clear quality control issues (syn2332184) were flagged as FAIL and were not included in downstream covariate analyses. For AltAnalyze analysis, unique putative novel exons were determined from all Tophat junction alignments in AltAnalyze version 2.0.9 and analyzed for associated exon-read coverage using the BedTools function BAMtoBED, along with all AltAnalyze predicted exons (Ensembl 72 and UCSC annotated mRNAs). The resulting exon.bed and junction.bed files for AltAnalyze were used as input for downstream statistical and visualization analyses (clustering, PCA and network analysis) in AltAnalyze, using indicated stringency options for transcription, exon and reciprocal junction analyses (syn3105745). For splicing visualization, coverage plots were produced from the Broad's IGV Sashimi-Plot function (Robinson et al., 2011). Protein isoform, protein domain and miRNA functional prediction algorithms are described in detail at http://www.altanalyze.org . Gene-level Fragment per Kilobase per Million (FPKM) expression estimates were also obtained with Cufflinks2 (Trapnell et al., 2012) using corrections for sequence-specific bias and multi-mapped reads (syn2247799). The specific parameters for both Tophat and Cufflinks are stored in provenance records in Synapse (see for example syn2246887). Gene-level expression estimates based on the Transcript per Million (TPM) estimates were additionally calculated using the software eXpress (Roberts and Pachter, 2013) for redistribution and comparative analysis (syn3033755).

miRNA-Seq Data Processing

miRNA expression was quantified with mirExpress v2.1.4 (Wang et al., 2009) using the human miRBase 20.0 reference (syn2247097). The counts for each miRNA were further filtered and normalized. Specifically the 2306 annotated miRNAs were filtered down to 1302 miRNAs that had at least two reads aligned in more than 10% of the samples. Each sample was then normalized by dividing the read counts by the count of the 90th percentile miRNA in each sample followed by standardization by mean and standard deviation. The quality of the data was assessed by PCA analysis and hierarchical clustering. Samples were considered FAIL with low overall annotated miRNA read-depth prior to normalization (syn2701942). Some samples were re-run and concatenated but ultimately not included in our analyses as these samples ultimately were more correlated to each other. Differentially expressed miRNAs were assessed using a series of linear models where expression was a function of tissue of origin, gender and reprogramming vector. All p-values were assessed using an f-test and corrected using Benjamini-Hochberg false discovery rate correction.

DNA-Methylation Data Processing

DNA-methylation arrays were normalized with the minfi R package (Aryee et al., 2014) (syn2233188). Before processing, a single cell line was removed due to a grossly abnormal karyotype and 12 other samples were removed due to poor intensity. The 12 samples had log2 median intensities for both methylated and unmethylated probes below 10.5. The remaining samples were quantile normalized.

CNV Analysis

The Plug-in cnvPartition (v3.2.0) for GenomeStudio was used to identify CNVs from the SNP arrays. For this software, the default settings were used, with the exception of a minimum loss of heterozygosity (changed to 5 Mb) and minimum number of SNPs (changed to 10).

Statistical Analyses

For pairwise comparison group analyses, a moderated t-test p-value (Smyth, 2004) was calculated for all pairwise comparisons by a custom python script between all major comparable metadata variables (syn2246673). This script uses existing methods available in the software AltAnalyze. It excludes samples with abnormal karyotypes for

analysis, can consider both unique donors and non-unique donors, will perform miRNA target enrichment analysis and miRNA differentially expressed comparison analysis, compare methylation and expression profiles via a Pearson correlation for matching samples, and optionally filters genes based on a priori selected expressed genes. Genes with a moderated t-test $p<0.05$, following a Benjamini-Hochberg adjustment and fold change >1.5 were considered differentially expressed when all samples were considered. To ensure the detected differences were biologically significant, differentially expressed genes and miRNAs were required to be expressed at least 20% the mean expression in hESC derived embryoid bodies. To evaluate potential regulation by methylation, genes and miRNAs with anticorrelated (Pearson rho<-0.5) expression from comparison of the same cell lines were furthered evaluated. As a secondary filtering method, genes, exons, miRNAs and probes with a non-adjusted $p<0.05$ for unique donors only (substantially smaller dataset) were considered reliably differentially expressed. Percent spliced in (PSI) ratios for any reciprocally expressed exon-exon junctions or introns and junctions were obtained using AltAnalyze and used as input for this script. Enrichment analyses of miRNA targets from differentially expressed genes were performed using GO-Elite (Zambon et al., 2012). In addition, DESeq2 (Love et al., 2014) was used to perform a multivariate analysis from read counts (HTSeq, syn2822494)(Anders et al., 2015) for all analyzed RNA-Seq samples (syn2838880).

Additional Results

Molecular Karyotypic Copy Number Variation (CNV) Analysis of iPSC

The largest number of clinically significant CNV were observed on chromosomes X and 15. Of interest, 12 of 16 female iPSC (75%), and 1 of 3 (33%) female hESC had low levels of X-chromosome monosomy observed in <10% of cells, regardless of cell type of origin, vector type or reprogramming gene combinations. Though it did not reach statistical significance, CNV were observed at higher frequency in lines generated using integrating vectors (retroviral and lentiviral vectors) with 7 of 12 lines (58%) carrying clinically significant CNV compared to 13 of 32 lines (41%) generated using non-integrating vectors ($p=0.37$; Fisher's Exact Test).

Seven unique donors were used in the generation of multiple lines, with each set of lines reprogrammed from the same cell type of origin. iPSC from five of these donors

also used the same reprogramming vector and could therefore be used to identify reprogramming associated CNV (donors D001,2,3,4 and 10) (Table S6). For example, all three lines reprogrammed from donor D003 had the same 719kb mosaic duplication at 15q11.2 indicating that it is likely present in the donor's originating somatic cells (SC11-008, 9 and 10). In contrast, CNV were more variable in the lines generated from donors D001, 2, 3, 4 and 9. Of interest, the three lines from donor D002 had divergent CNV calls. One line (SC11-005) had duplications in both 20q11.21 and 6q21, another line (SC11-006) had only the duplication in 20q11.21, and the third line (SC11-007) had only the 6q21 duplication. This suggests that both duplications pre-existed in the original donor cells and were preserved in SC11-005, but one was lost in each of the other two lines. Overall, this indicates some level of instability in the lines from this donor.

References

Anders, S., Pyl, P.T., and Huber, W. (2015). HTSeq-a Python framework to work with high-throughput sequencing data. Bioinformatics *31*, 166-169.

Aryee, M.J., Jaffe, A.E., Corrada-Bravo, H., Ladd-Acosta, C., Feinberg, A.P., Hansen, K.D., and Irizarry, R.A. (2014). Minfi: a flexible and comprehensive Bioconductor package for the analysis of Infinium DNA methylation microarrays. Bioinformatics *30*, 1363-1369.

Emig, D., Salomonis, N., Baumbach, J., Lengauer, T., Conklin, B.R., and Albrecht, M. (2010). AltAnalyze and DomainGraph: analyzing and visualizing exon expression data. Nucleic acids research *38*, W755-762.

Encode Project Consortium (2012). An integrated encyclopedia of DNA elements in the human genome. Nature *489*, 57-74.

Kim, D., Pertea, G., Trapnell, C., Pimentel, H., Kelley, R., and Salzberg, S.L. (2013). TopHat2: accurate alignment of transcriptomes in the presence of insertions, deletions and gene fusions. Genome biology *14*, R36.

Love, M.I., Huber, W., and Anders, S. (2014). Moderated estimation of fold change and dispersion for RNA-seq data with DESeq2. Genome biology *15*, 550.

Purcell, S., Neale, B., Todd-Brown, K., Thomas, L., Ferreira, M.A., Bender, D., Maller, J., Sklar, P., de Bakker, P.I., Daly, M.J.*, et al.* (2007). PLINK: a tool set for whole-genome association and population-based linkage analyses. American journal of human genetics *81*, 559-575.

Roberts, A., and Pachter, L. (2013). Streaming fragment assignment for real-time analysis of sequencing experiments. Nature methods *10*, 71-73.

Robinson, J.T., Thorvaldsdottir, H., Winckler, W., Guttman, M., Lander, E.S., Getz, G., and Mesirov, J.P. (2011). Integrative genomics viewer. Nature biotechnology *29*, 24-26.

Rosenbloom, K.R., Armstrong, J., Barber, G.P., Casper, J., Clawson, H., Diekhans, M., Dreszer, T.R., Fujita, P.A., Guruvadoo, L., Haeussler, M.*, et al.* (2014). The UCSC Genome Browser database: 2015 update. Nucleic acids research.

Smith, B., Ashburner, M., Rosse, C., Bard, J., Bug, W., Ceusters, W., Goldberg, L.J., Eilbeck, K., Ireland, A., Mungall, C.J.*, et al.* (2007). The OBO Foundry: coordinated evolution of ontologies to support biomedical data integration. Nature biotechnology *25*, 1251-1255.

Smyth, G.K. (2004). Linear models and empirical bayes methods for assessing differential expression in microarray experiments. Statistical applications in genetics and molecular biology *3*, Article3.

Thomson, J.A., Itskovitz-Eldor, J., Shapiro, S.S., Waknitz, M.A., Swiergiel, J.J., Marshall, V.S., and Jones, J.M. (1998). Embryonic stem cell lines derived from human blastocysts. Science *282*, 1145-1147.

Trapnell, C., Roberts, A., Goff, L., Pertea, G., Kim, D., Kelley, D.R., Pimentel, H., Salzberg, S.L., Rinn, J.L., and Pachter, L. (2012). Differential gene and transcript expression analysis of RNA-seq experiments with TopHat and Cufflinks. Nature protocols *7*, 562-578.

Whetzel, P.L., and Team, N. (2013). NCBO Technology: Powering semantically aware applications. Journal of biomedical semantics *4 Suppl 1*, S8.

Zambon, A.C., Gaj, S., Ho, I., Hanspers, K., Vranizan, K., Evelo, C.T., Conklin, B.R., Pico, A.R., and Salomonis, N. (2012). GO-Elite: a flexible solution for pathway and ontology over-representation. Bioinformatics *28*, 2209-2210.

Supplemental Figures

Figure S1, related to Figure 1: Standardized Preliminary Screening of iPSC lines. A) Normal female karyotype for SC11-010. B) Abnormal female karyotype for SC11-003 with 47,XX, del(8)p23,+12. C) Immunohistological staining with anti-OCT4 antibody of a teratoma with a poorly differentiated area that is confirmed to have undifferentiated cells by SC12-034. Histopathological analysis of Teratomas from iPSC line with representatives of D) mesoderm, endoderm and ectoderm. Immunohistological analysis of a teratoma from SC12-025 with E) OCT4, F) Alpha-feto protein, G) Neurofilament, and H) Muscle Specific Actin staining.

Figure S2, related to Figure 2: Copy Number Variation Analyses. A) Summary CNV by reprogramming vector (n=50). Bars in blue show non-benign CNV and in red show clinically significant CNV. Benign CNV are not shown. B) The mean of clinically significant CNV in hESC, iPSC generated with non-integrating or integrating vectors. None of the comparisons were significantly different by student's t-test: blastocyst vs integrating, p= 0.0891, integrating vs non-integrating, p=0.1734, blastocyst vs non-integrating, p=0.2405 (2-tailed, heteroscedastic). C) Non-Benign CNV partially observed in at least one of two iPSC from a single donor are shown.

Figure S3, related to Figure 3: Global Similarity of iPSC and hESC. A) Hierarchical clustering of gene expression differences present among hESC, iPSC and hESC derived EB by RNA-Seq. Genes with a 4 fold difference between at least 8 samples and correlated (rho>0.5 or rho<-0.5) with the expression of at least 10 other genes are shown. This filtering schema was used to enrich for differentially expressed genes with similar expression patterns that are shared across multiple lines. Relative expression calculated to the average of the EB and iPSC average expression for each gene. A singular value decomposition (SVD) analysis of the top three principal components for all RNA-Seq genes with a minimum RPKM of 5 and at least 500 reads/gene (n=5801) are displayed to the right of the heatmap. The same analysis workflow was run on B) DNA-methylation profiles with at least 3 samples with beta values less than 0.33 and at least 3 samples greater than 0.66 and C) microRNA-seq expression profiles with at least 50 reads per microRNA, to obtain correlated/anticorrelated probe or microRNA clusters. PCA plots were generated from the initial filtered sets, before correlated clusters were selected.

Detailed cell line data and expression values can be found in synapse: https://www.synapse.org/#!Synapse:syn1773109/files/

Figure S4, related to Figure 4: Global and Representative Reprogramming Specific Molecules. (A) Top-ranking DNA-methylation probes and corresponding genes for representative unique donor samples. Shapes are distinct by covariate. Anticorrelated gene expression and DNA-methylation are indicated by a red alpha and significant differentially expressed genes by an asterisk. B) The top ranking differentially expressed genes by pairwise comparison p-value for reprogramming associated variables extracted from the cell line metadata for representative unique donor samples. Measurements in red indicate the same parental genetic donor (D007). C) Correlated qPCR (TLDA) and RNA-Seq Gene Expression Profiles. Gene expression normalized to the mean of all evaluated pluripotent stem cells and single embryoid body are shown for the top 4 most correlated genes between TLDA and RNA-Seq.

Figure S5, related to Figure 5: Alternative Splicing Events. A) Hierarchical clustering of the top-ranking alternative splicing events for hESC versus EB. Values are reported as percent spliced in (PSI) from AltAnalyze normalized to the average of the hESC and EB average PSI. White indicates no PSI calculated due to insufficient detection of RNA isoforms for the indicated splicing events (drop-outs). B) Top reprogramming associated splicing events for representative unique donor samples.

Figure S6, related to Figure 6: Sex-Associated Autosomal DNA-Methylation. A) Previously proposed X-chromosome inactivation specific Illumina 450k DNA-Methylation probes (n=3,279, Nazor et. al Cell Stem Cell 2012) and associated gene expression profiles. B) Unsupervised hierarchical clustering of the top differentially methylated autosomal methylation probes, filtering for any probe with at least one sample containing less than 0.3 beta and at least one other sample with greater than 0.6 beta (n=22,678). Probe cluster annotations are indicated below the heatmap. C) Biologically enriched (Benjamini-Hochberg adjusted $p<0.05$) categories from ToppGene corresponding to the 10 reported clusters from B) visualized in Cytoscape. D) DNA-methylation beta values for lineage directing transcription factors in high and low *XIST* female iPSC. E) Representative genes with expression anti-correlated to multiple measures of XCI in definitive endoderm (DE), mesoderm (Meso) and ectoderm (Ecto) directed differentiations of female PSC. F) Comparison of high and low *XIST* PSC derived teratomas based on the percent

positive quantification of muscle specific actin (MSA) or neurofilament (NF) staining.

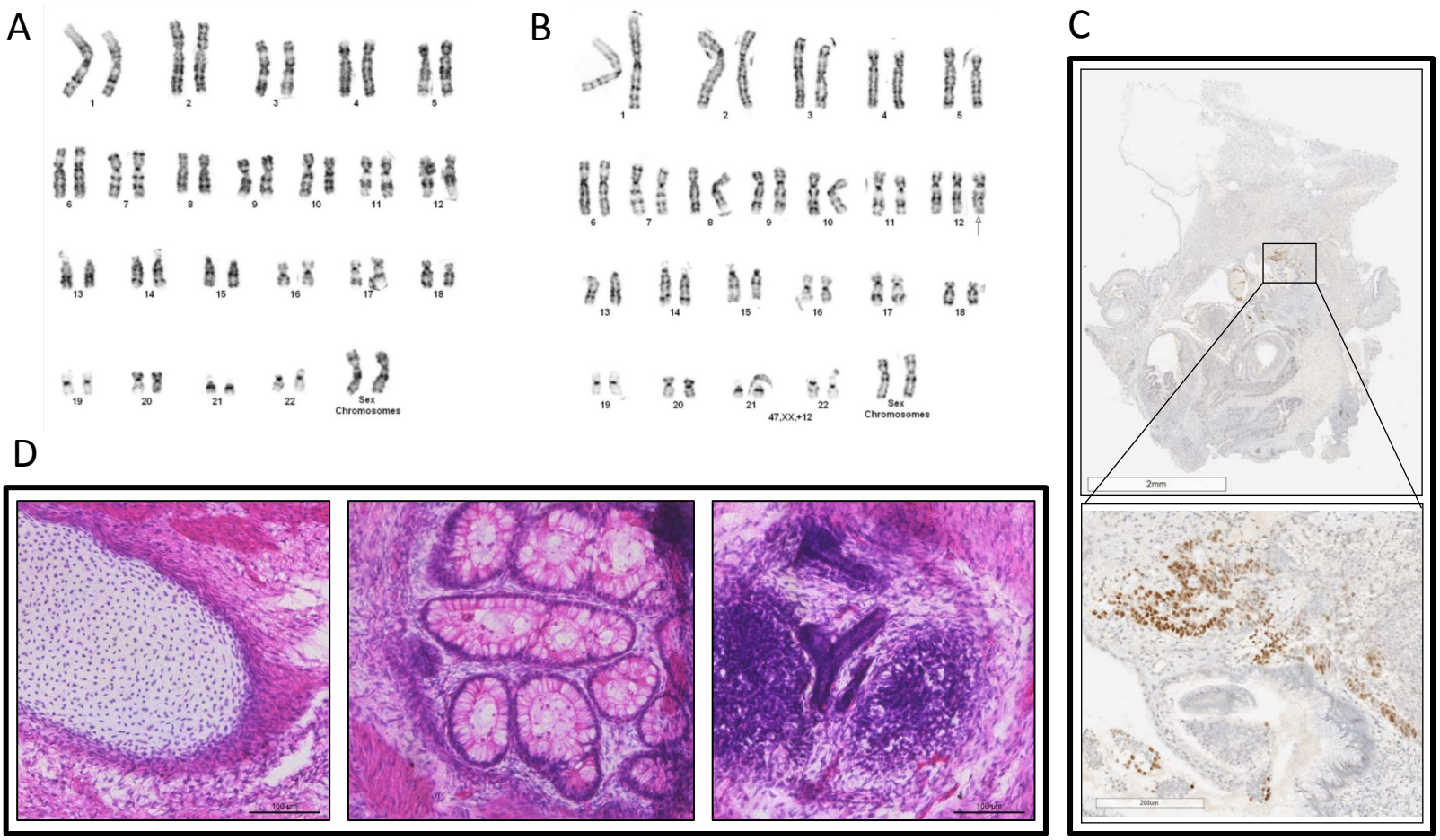
A
B
C
D
E
F
G
H
Sex Chromosomes
47,XX,+12
2mm
100 μm
200um
300um

Supplemental Figure 2

A

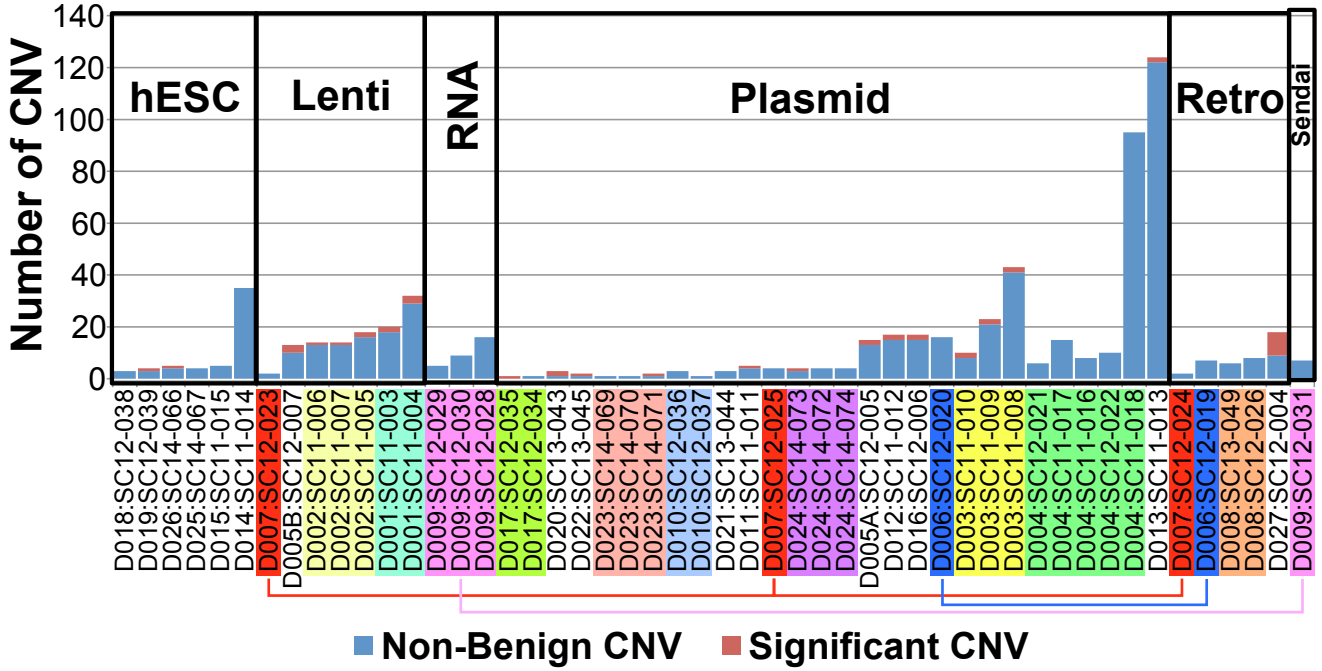

B

Summary of CNV by vector type.

Vector	Sig CNV	N	Mean Significant CNV	Standard Error	Range
Blastocyst	2	6	0.33	0.210819	0-1
Non-Integrating	21	28	0.75	0.73983	0-2
Integrating	21	12	1.75	0.15299	0-9

C

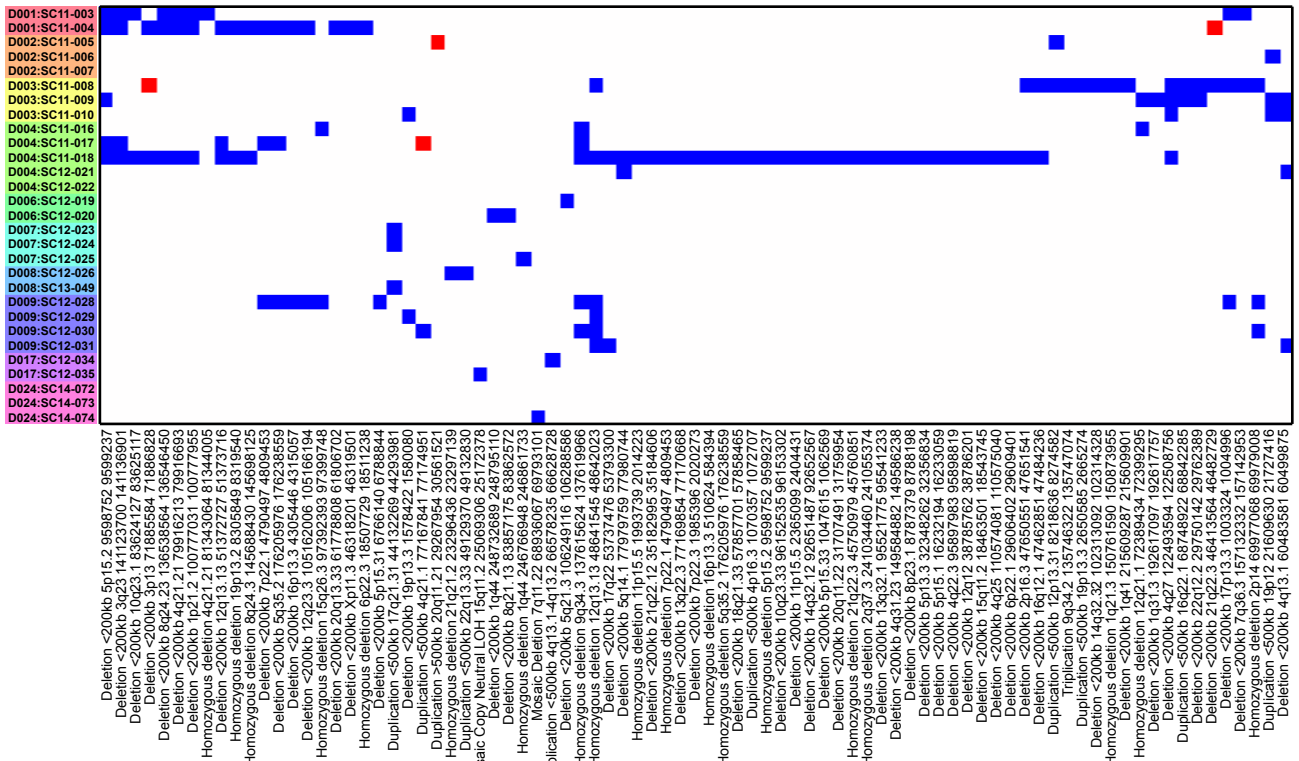

Supplemental Figure 3

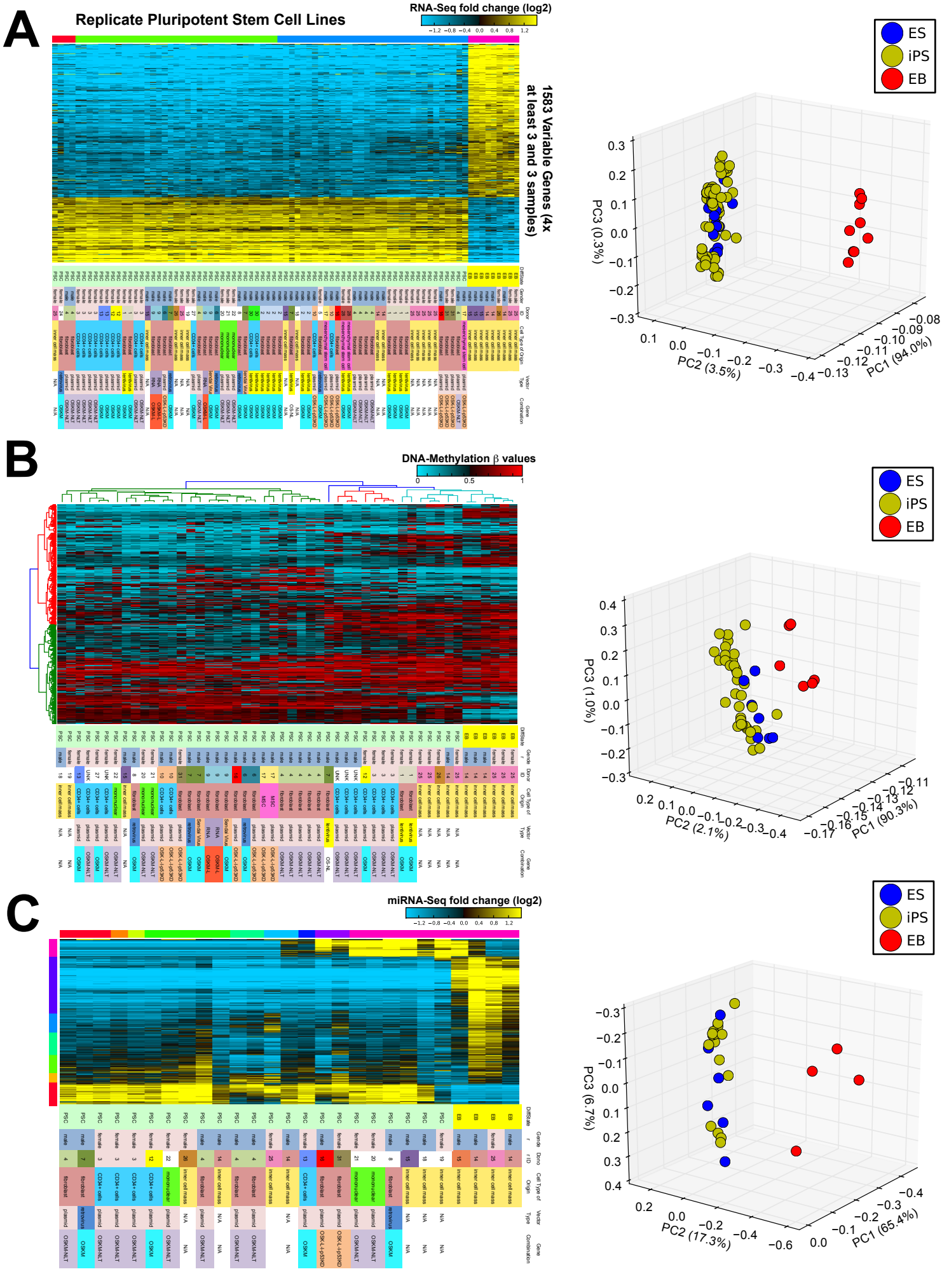

Supplemental Figure 4

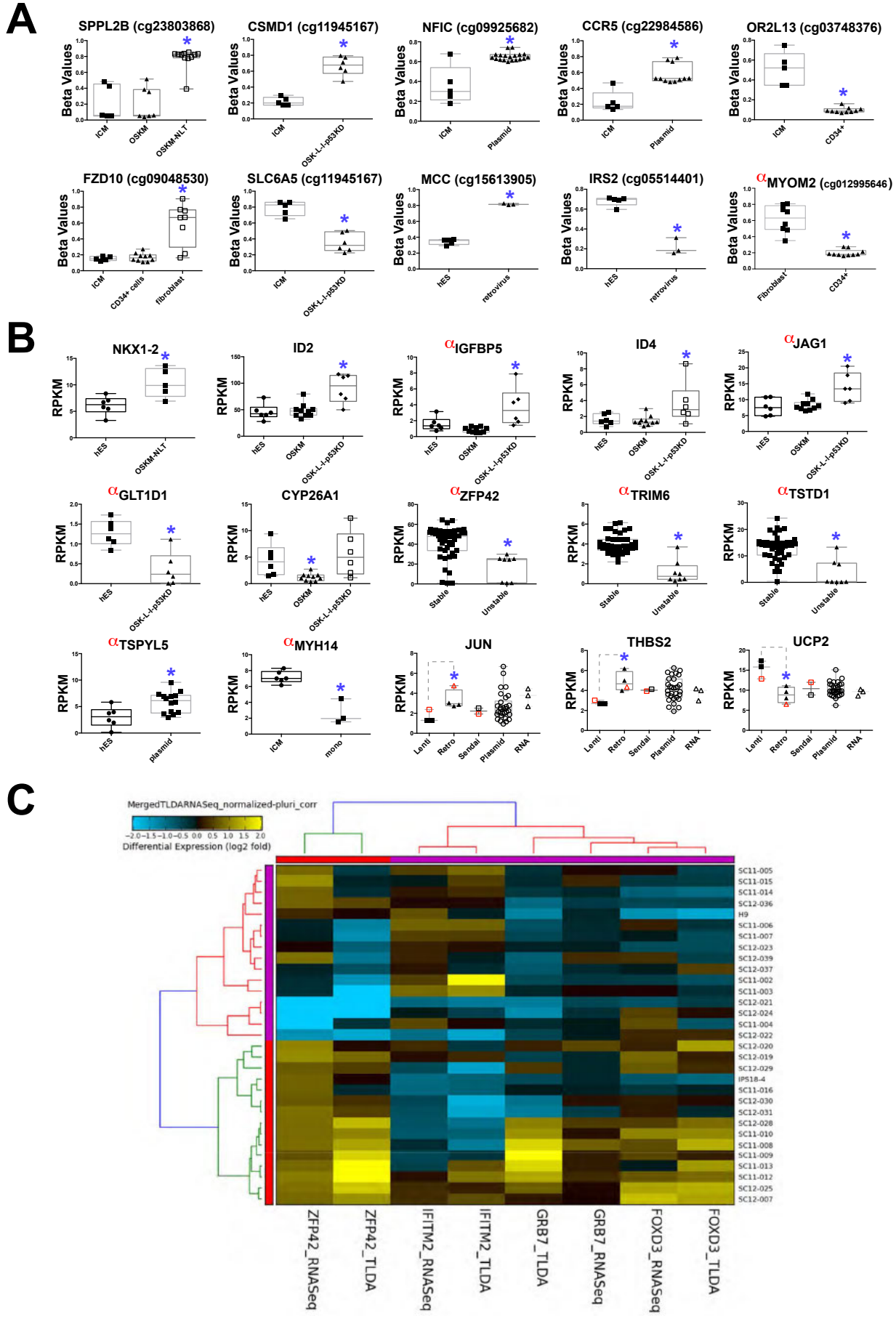

Supplemental Figure 5

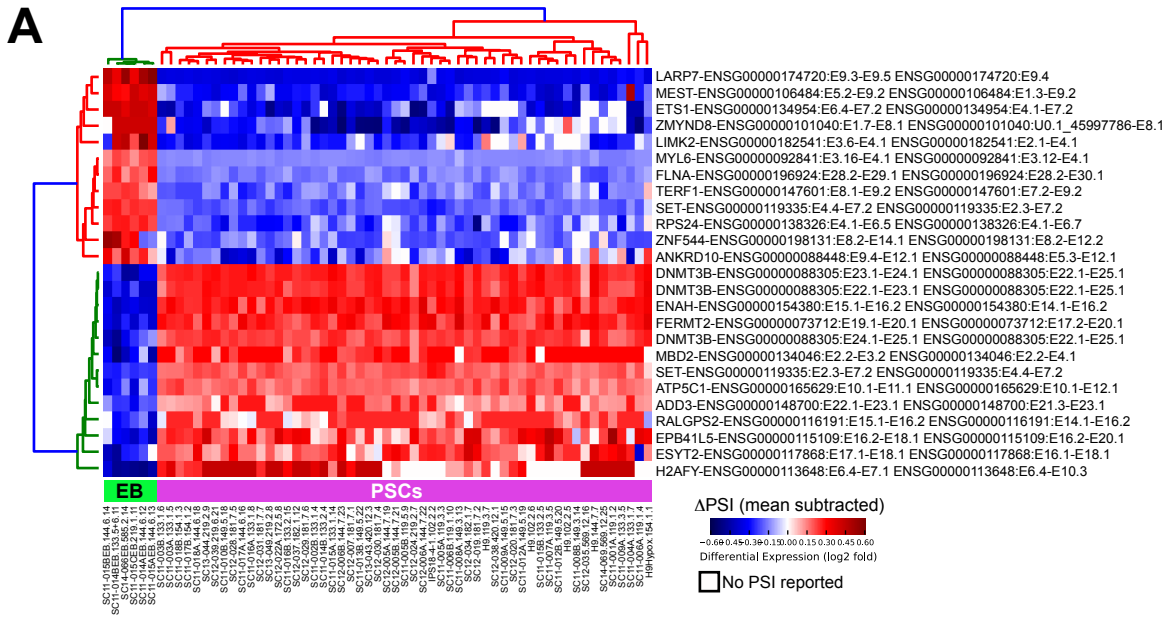

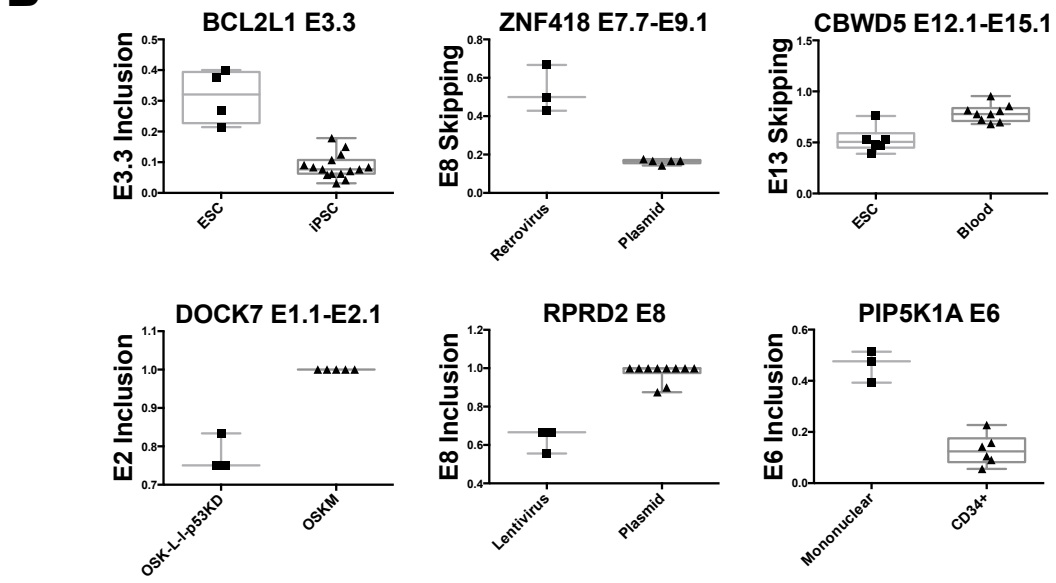

Supplemental Figure 6

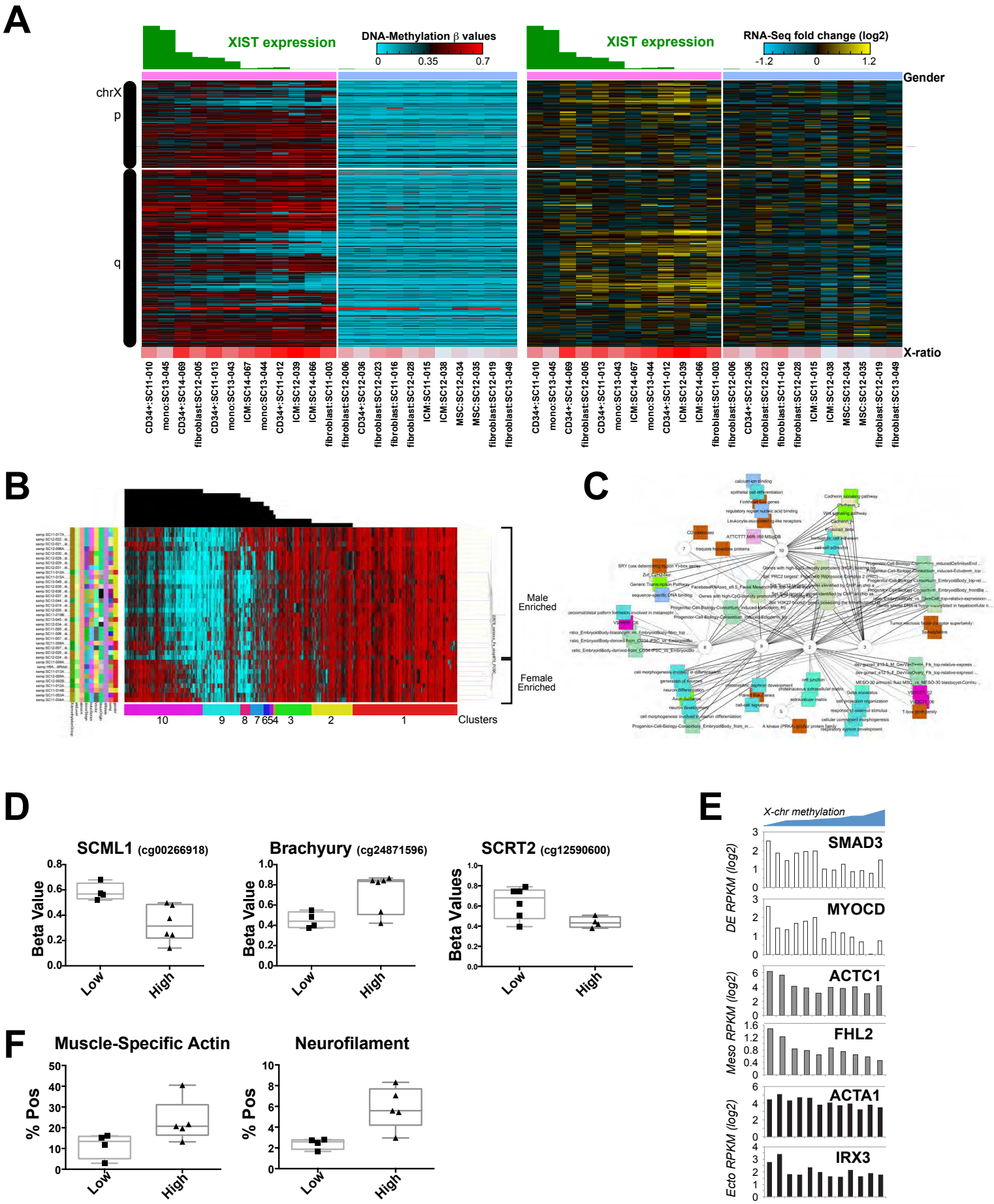

Supplementary Table 1: Cell line nomenclature, contributors and references (if previously published).

PCBC Cell Line Name	C4 Cell Line ID	Originating Lab ID	Principle Investigator	Other Significant Contributor	PMID or other reference info
PCBC01hsi2011070101	SC11-002	CHOP_WT1.1	Weiss, Gadue, & French	Jason A Mills	PMCID: 3778548
PCBC01hsi2011070102	SC11-003	CHOP_WT1.2	Weiss, Gadue, & French	Jason A Mills	PMCID: 3778548
PCBC01hsi2011070103	SC11-004	CHOP_WT1.3	Weiss, Gadue, & French	Jason A Mills	PMCID: 3778548
PCBC01hsi2011070104	SC11-005	CHOP_WT2.1	Weiss, Gadue, & French	Jason A Mills	PMCID: 3778548
PCBC01hsi2011070105	SC11-006	CHOP_WT2.2	Weiss, Gadue, & French	Jason A Mills	PMCID: 3778548
PCBC01hsi2011070106	SC11-007	CHOP_WT2.3	Weiss, Gadue, & French	Jason A Mills	PMCID: 3778548
PCBC03hsi2011080401	SC11-008	CBiPS-6.2	Elias Zambidis	N/A	PMCID: PMC3072973
PCBC03hsi2011080402	SC11-009	CBiPS-19.11	Elias Zambidis	N/A	PMCID: PMC3072973
PCBC03hsi2011080403	SC11-010	CBiPS-6.13	Elias Zambidis	N/A	PMCID: PMC3072973
PCBC03hsi2011080404	SC11-011	CBiPS-E5C3	Elias Zambidis	Tea Soon Park	PMCID: PMC3414503
PCBC03hsi2011080405	SC11-012	CBiPS-E12C1	Elias Zambidis	Tea Soon Park	PMCID: PMC3414503
PCBC03hsi2011080406	SC11-013	CBiPS-E17C6	Elias Zambidis	Tea Soon Park	PMCID: PMC3414503
PCBC02hse2011100705	SC11-014	WA01	James Thomson	N/A	9804556
PCBC02hse2011100706	SC11-015	WA24	James Thomson	N/A	9804556
PCBC02hsi2011100701	SC11-016	DF19-9-7T/DF19.7	James Thomson	Junying Yu	19325077
PCBC02hsi2011100703	SC11-017	DF4-3-7T.A/DF4.7	James Thomson	Junying Yu	19325077
PCBC02hsi2011100702	SC11-018	DF6-9-9T.B/DF6.9	James Thomson	Junying Yu	19325077
PCBC15hsi2011102602	SC12-003	virWTb	Bruce Conklin	Shiro Baba	PMID: 24509632, PMC4063274
PCBC15hsi2011102603	SC12-004	virWTa	Bruce Conklin	Shiro Baba	PMID: 24509632, PMC4063274
PCBC15hsi2012040401	SC12-005	epiWTb	Bruce Conklin	Yohei Hayashi	PMID: 24509632, PMC4063274
PCBC15hsi2012040402	SC12-006	epiWTc	Bruce Conklin	Yohei Hayashi	PMID: 24509632, PMC4063274
PCBC15hsi2012062201	SC12-007	virWTb	Bruce Conklin	Shiro Baba	PMID: 24509632, PMC4063274
PCBC05hsi2012061401	SC12-019	HFF12	Beverly Torok-Storb	Aravind Ramakrishnan	N/A
PCBC05hsi2012061402	SC12-020	niPSC	Beverly Torok-Storb	Aravind Ramakrishnan	N/A

PCBC02hsi2011100704	SC12-021	mND1	James Thomson	Guokai Chen	21478862
PCBC02hsi2012082101	SC12-022	MIRJT7-mND2-0-WB0119	James Thomson	Guokai Chen	21478862
PCBC16hsi2011111501	SC12-023	lenti-8.4.1	Jonathan Slack	Lucas V. Greder, James Dutton	23197849
PCBC16hsi2011111502	SC12-024	retro-20.1	Jonathan Slack	Lucas V. Greder, James Dutton	N/A
PCBC16hsi2011111503	SC12-025	Sendai-9-1	Jonathan Slack	Lucas V. Greder, James Dutton	23326500, 24485793
PCBC16hsi2011081101	SC12-026	kyba029	Michael Kyba	Abhijit Dandapat, Jakub Tolar	N/A
PCBC08hsi2012082303	SC12-027	BJ Epi 5	George Daley, Thorsten Schlaeger	Alexander DeVine	N/A
PCBC08hsi2012082304	SC12-028	BJ RiPS 1	George Daley, Thorsten Schlaeger	Andrew ttenger	N/A
PCBC08hsi2012082305	SC12-029	BJ RiPS 2	George Daley, Thorsten Schlaeger	Andrew ttenger	N/A
PCBC08hsi2012082306	SC12-030	BJ RiPS 3	George Daley, Thorsten Schlaeger	Andrew ttenger	N/A
PCBC08hsi2012082310	SC12-031	BJ Sendai 1	George Daley, Thorsten Schlaeger	Kelly Fitzgerald	N/A
PCBC08hsi2012082311	SC12-032	BJ Sendai 2	George Daley, Thorsten Schlaeger	Kelly Fitzgerald	N/A
PCBC08hsi2012082312	SC12-033	BJ Sendai 3	George Daley, Thorsten Schlaeger	Kelly Fitzgerald	N/A
PCBC08hsi2012082315	SC12-034	haMSC 17	George Daley, Thorsten Schlaeger	Fauza, Alexander DeVine	N/A
PCBC08hsi2012082316	SC12-035	haMSC 18	George Daley, Thorsten Schlaeger	Fauza, Alexander DeVine	N/A
PCBC08hsi2012082318	SC12-036	CD34+ 1	George Daley, Thorsten Schlaeger	Colin Sieff, Kelly Fitzgerald	N/A
PCBC08hsi2012082319	SC12-037	CD34+ 2	George Daley, Thorsten Schlaeger	Colin Sieff, Kelly Fitzgerald	N/A
PCBC08hse2012100901	SC12-038	CHB4	George Daley	Paul Lerou	18223642
PCBC08hse2012100902	SC12-039	CHB8	George Daley	Paul Lerou	18223642
PCBC10hsi2012051001	SC12-040	BJ iPSC	John Cooke	Sheena Abraham, Eduard Yakubov	N/A
PCBC02hsi2012090602	SC13-043	IISH1i-BM1	Igor Slukvin	Kejin Hu	21296996
PCBC02hsi2012090601	SC13-044	IISH2i-BM9	Igor Slukvin	Kejin Hu	21296996
PCBC02hsi2012090603	SC13-045	IISH3i-CB6	Igor Slukvin	Kejin Hu	21296996
PCBC16hsi2013040201	SC13-049	029 iPS clone 4	Michael Kyba	Abhijit Dandapat, Jakub Tolar	N/A
PCBC03hsi2013090602	SC13-059	E20C2	Elias Zambidis	Tea Soon Park	PMCID: PMC3414503

PCBC03hsi2013090603	SC13-060	E24C2	Elias Zambidis	Tea Soon Park	PMCID: PMC3414503
PCBC03hsi2013090604	SC13-061	E17C1	Elias Zambidis	Tea Soon Park	PMCID: PMC3414503
PCBC03hsi2013090605	SC13-062	E32C9	Elias Zambidis	Tea Soon Park	PMCID: PMC3414503
PCBC03hsi2013090606	SC13-063	E7C1	Elias Zambidis	Tea Soon Park	PMCID: PMC3414503
PCBC03hsi2013090607	SC13-064	E7C9	Elias Zambidis	Tea Soon Park	PMCID: PMC3414503
PCBC03hsi2013090608	SC13-065	E7C12	Elias Zambidis	Tea Soon Park	PMCID: PMC3414503
PCBC02hse2014030501	SC14-066	WA07	James Thomson	N/A	9804556
PCBC02hse2014030502	SC14-067	WA09	James Thomson	N/A	9804556
PCBC03hsi2014031101	SC14-069	4F CB-iPSC-MSC, LZ6-1	Elias Zambidis	Ludovic Zimmerlin	N/A
PCBC03hsi2014031102	SC14-070	4F CB-iPSC-MSC, LZ6-2	Elias Zambidis	Ludovic Zimmerlin	N/A
PCBC03hsi2014031103	SC14-071	4F CB-iPSC-MSC, LZ6-12	Elias Zambidis	Ludovic Zimmerlin	N/A
PCBC03hsi2014031104	SC14-072	4F CB-iPSC-MSC, LZ6+2	Elias Zambidis	Ludovic Zimmerlin	N/A
PCBC03hsi2014031105	SC14-073	4F CB-iPSC-MSC, LZ6+3	Elias Zambidis	Ludovic Zimmerlin	N/A
PCBC03hsi2014031106	SC14-074	4F CB-iPSC-MSC, LZ6+10	Elias Zambidis	Ludovic Zimmerlin	N/A

Supplementary Table 2: List of Assays Used to Characterize iPSC

Preliminary Assays
Colony and cellular morphology
Sterility
Mycoplasma
Flow cytometry (SSEA-1,SSEA-4, TRA-1-61, TRA-1-80, CD9, OCT-4)
Karyotype
Comprehensive Assays
RNA-seq
mi-RNA seq
dna methylation (450K CpG)
copy number variation (SNP)
Stem Cell Gene RT-PCR Expression Panel TLDA - 92 genes
Teratoma with Histopathological Analysis

!

Supplementary Table 3: Criteria for a line to be designated as stable.

Assay	Result	
Morphology	Normal	
Sterility (14 days)	No growth	
Mycoplasma	No mycoplasma	
Karyotype	20 of 20 [46,XY or XX]	
Flow Cytometry Analysis Self-Renewal Markers	SSEA-4	>95%
	TRA-1-60	>85%
	TRA-1-81	>85%
	OCT-4	>90%
	CD9	>90%
Flow Cytometry Analysis Differentiation Marker	SSEA-1	<5%

Supplementary Table 4: Summary of rationale for unstable lines determination and/or line not eligible for complete analysis.

Assay	Number of lines (%)
Non-Sterile	0
Mycoplasma Contamination	6 (9%)
Flow cytometry profile and/or differentiated morphology	6 (9%)
Abnormal Karyotype	7 (11%)
Quarantine	4 (6%)

Supplementary Table 5: Summary of karyotype abnormalities in iPSC lines.

Cell Line	Karyotype	Additional Information for Complex Karyotypes	Sex	Cell of Origin	Vector Type	Genes
SC11-002	47, XX, +12 [2] / 46, XX [18]		Female	fibroblast	lenti (Cre-excised)	OSKM
SC11-003	47, XX, +12 [15] / 47, XX, idem, del 8p23 [2] / 46, XX [2]	2 cells normal, 1 cell trisomy 5 (non-clonal), 17 cells trisomy 12, of those 17, 2 cells have a deletion at 8p23	Female	fibroblast	lenti (Cre-excised)	OSKM
SC12-003	46, XX [49]/ 47, XX +12 [1]		Female	fibroblast	retro	OSKM
SC12-004	46, XY, add 1q21	All 20 cells have material of unknown origin added to 1q21, creating a functional monosomy for distal 1q and partial trisomy for the region of genome added to 1q.	Male	fibroblast	retro	OSKM
SC12-026	47, XYY [2] / 46, XY [18]		Male	fibroblast	retro	OSKM
SC12-040	65-71,XXX,+add(X)(q28)[9],add(1)(q32)x2,-2[6],add(2)(q25)[3],add(3)(p13),add(3)(q21),-4[4],add(4)(21)[6],+6[7],-7[4],-9[8],add(9)(q22)[3],+10[4],+10[2],+12[2],-13,add(13)(p11.1),-14[3],-15[9],-15[3],-16[4],+17[7],add(17)(p11.2)[8],add(18)(q22)[8],20[3],+21[5],add(21)(22)[5],i(21)(q10)x2,+22[6],add(22)(11.2)[6],+mar1[8],+mar2[3],+1-2mar[9][cp10]	10 of 10 cells	Female	fibroblast	mRNA	OSKM
SC12-033	48, XY, +12, +20[2]/46, XY[37]		Male	BJ fibroblast	Sendai Vector	OSKM

Supplementary Table 6: Comparison of the CNV detected among the iPSC lines generated from common donors.

Unique Donor	Sex	Cell of origin	Vector	Genes	iPSC Line	Clinically Significant CNV
D001	Female	fibroblast	lenti	OSKM	SC11-003	low level mosaic monosomy for Xp22.33-Xq28
						interstitial duplication of 1.3Mb of 7q11.22
					SC11-004	interstitial duplication of 1.2Mb from 5q34
						interstitial duplication of 1.3Mb from 3q26.31
						low level mosaic monosomy for Xp22.33-Xq28
D002	Male	fibroblast	lenti	OSKM	SC11-005	1.3 Mb duplication at 20q11.21
						941Kb duplication at 6q21
					SC11-006	2.15 Mb Mosaic Duplication at 20q11.21
					SC11-007	1.69 Mb bp duplication at 6q21
D003	Female	UCB CD34+	plasmid	OSKM - NLT	SC11-008	719Kb Mosaic Duplication at 15q11.2
						Mosaic monosomy at Xp22.33-Xq28
					SC11-009	719Kb Mosaic Duplication at 15q11.2
						Mosaic monosomy at Xp22.33-Xq28
					SC11-010	719Kb Mosaic Duplication at 15q11.2
						Mosaic monosomy at Xp22.33-Xq28
D004	Male	fibroblast	plasmid	OSKM - NLT	SC11-016	No clinically significant chr imbalances
					SC11-017	No clinically significant chr imbalances
					SC11-018	No clinically significant chr imbalances
					SC12-021	No clinically significant chr imbalances
					SC12-022	No clinically significant chr imbalances
D007	Male	fibroblast	lenti	OS-NL	SC12-023	No clinically significant chr imbalances
			Retro	OSKM	SC12-024	No clinically significant chr imbalances
			plasmid	OSKM	SC12-025	No clinically significant chr imbalances
D009	Male	fibroblast	mRNA	OSKM-L	SC12-028	No clinically significant chr imbalances
			mRNA	OSKM-L	SC12-029	No clinically significant chr imbalances
			RNA	OSKM-L	SC12-030	No clinically significant chr imbalances
			Sendai Virus	OSKM	SC12-031	No clinically significant chr imbalances
D010	Male	BM CD34+	Episomal	OSK-L-I-p53KD	SC12-036	No clinically significant chr imbalances
				OSK-L-I-p53KD	SC12-037	No clinically significant chr imbalances

Supplememtary Table 7: Immunostaining analysis of teratomas generated from PSC lines with differentiated morphology in culture and independent control lines generated from the same donors.

Cell Line	PSC culture morphology	Donor ID	Cell Type	MSA	NF	AFP	OCT4	histopathologic analysis summary	Teratoma interpretation
SC12-021	Spontaneous differentiation	4	iPSC	+++	+	+++	-	Well differentiated pluripotent teratoma	Within the cut section of the tumor, there is benign well differentiated teratoma composed of solid and cystic areas and contain tissue types arising from all three primordial germ cell layers. Solid areas are composed of mixed population of moderately cellular neural tissue with glial cells and smaller primitive neuroepithelial cells in a background of neurofibrillary material interspersed by cartilage. In few places, solid areas are contain numerous columnar cells that frequently form glands and acini consistent with sebaceous glands. Cysts are lined by variety of cells ranging from cuboidal to simple columnar with multifocal cilia. There are many goblet cells are present in some cysts. Some cysts are lined by columnar epithelium with occasional cilia and interspersed with goblet cells (putative respiratory epithelium). Some cysts contain columnar epithelium that frequently folds into villi like structures with few goblet cells (putative intestine)
SC12-022	Undifferentiated	4	iPSC	++	++	+++	-	Well differentiated pluripotent teratoma	Within the cut section of the tumor, there is benign well differentiated teratoma composed of solid and cystic areas and contain tissue types arising from all three primordial germ cell layers. Solid areas are composed primarily of moderately cellular neural tissue with glial cells and smaller primitive neuroepithelial cells in a background of neurofibrillary material. Additional solid tissue include cartilaginous tissue. Cysts are lined by a variety of epithelial cells, ranging from squamous to cuboidal to simple and pseudostratified columnar with multifocal cilia. Few to many goblet cells are present in some cysts. Some cysts contain eosinophilic to amphophilic amorphous to fibrillar material.
SC12-023	Spontaneous differentiation	7	iPSC	+++	+	+	-	Well differentiated pluripotent teratoma	Within the cut section of the tumor, there is benign well differentiated teratoma composed of solid and cystic areas and contain tissue types arising from all three primordial germ cell layers. Solid areas are composed of mixed population of moderately cellular neural tissue with glial cells and smaller primitive neuroepithelial cells in a background of neurofibrillary material. Cysts are lined by variety of cells ranging from cuboidal to simple columnar with multifocal cilia. There are many goblet cells are present in some cysts. These cysts are vary from being respiratory epithelium to digestive tract epithelium.
SC12-025	Undifferentiated	7	iPSC	++	+	++	+ (a few small positivite columnar epithelial cells)	Well differentiated pluripotent teratoma	Within the cut section of the tumor, there is benign well differentiated teratoma composed of solid and cystic areas and contain tissue types arising from all three primordial germ cell layers. Solid areas are composed of mixed population of moderately cellular neural tissue with glial cells and smaller primitive neuroepithelial cells in a background of neurofibrillary material admixed with cartilage. Cysts are lined by variety of cells ranging from cuboidal to simple columnar with multifocal cilia. There are many goblet cells are present in some cysts. These cysts represent variety of putative differentiated tissues ranging from intestine, hair follicle, skin and respiratory epithelium. Frequently these cysts appear mixture of differentiated tissues containing eosinophilic to amphophilic amorphous to fibrillar material and occasionally keratin in lumen.
SC14-082	Spontaneous differentiation	unique	iPSC	ND	ND	ND	ND	Well differentiated pluripotent teratoma	Within the cut section of the tumor, there is benign well differentiated teratoma composed of solid and cystic areas and contain tissue types arising from all three primordial germ cell layers. Solid areas are composed primarily of moderately cellular neural tissue with glial cells and smaller primitive neuroepithelial cells in a background of neurofibrillary material. Additional solid tissue include cartilage, bone, hair, teeth and structures resembling acini glands. Cysts are lined by a variety of epithelial cells, ranging from squamous to cuboidal to simple and pseudostratified columnar with multifocal cilia. Few to many goblet cells are present in some cysts. Some cysts contain eosinophilic to amphophilic amorphous to fibrillar material.

Supplememtary Table 8: Immunostaining of teratomas with histopathologically identified undifferentiated regions and control teratomas generated from the same PSC line

Cell Line	PSC culture morphology	Donor ID	Cell Type	MSA	NF	AFP	OCT4	Teratoma histopathologic analysis	Teratoma Interpretation
SC12-034	Undifferentiated	17	iPSC	+++	++	++	++ (a few small strong OCT4 areas)	Poorly differentiated areas within one teratoma	Within the cut section of the tumor, there is benign well differentiated teratoma composed of solid and cystic areas and contain tissue types arising from all three primordial germ cell layers. Solid areas are composed of mixed population of moderately cellular neural tissue with glial cells and smaller primitive neuroepithelial cells in a background of neurofibrillary material. Multifocally, there are numerous capillaries frequently filled with erythrocytes. There are numerous cysts are lined by variety of cells ranging from simple columnar to stratified squamous epithelium. These cysts are vary from being digestive tract epithelium to skin.
SC12-034	Undifferentiated	17	iPSC	++	+	++	-	Well differentiated pluripotent teratoma	Within the cut section of the tumor, there is a benign cystic spaces that are lined by variety of cells ranging from cuboidal to simple squamous epithelium. These cystic spaces occasionally have mucin like material in the lumen. Majority of the solid space is composed of neuronal tissue and loosely arranged mesenchymal tissue. Part of the solid tissue components include primitive tooth like structures, cartilage and transitional epithelium.
SC11-013	Undifferentiated	13	iPSC	+	+	++	-	Well differentiated pluripotent teratoma	Within the cut section of the tumor, there is benign well differentiated teratoma composed of solid and cystic areas and contain tissue types arising from all three primordial germ cell layers. Solid areas are composed primarily of moderately cellular neural tissue with glial cells and smaller primitive neuroepithelial cells in a background of neurofibrillary material. Additional solid tissue include cartilaginous tissue. Cysts are lined predominantly by cuboidal to simple columnar with multifocal cilia. There are few goblet cells are present in some cysts.
SC11-013	Undifferentiated	13	iPSC	+	+	+	-	Poorly differentiated teratoma	Within the cut section of the tumor, there is benign poorly differentiated teratoma composed of solid (predominant) and cystic areas. There is no identifiable mesodermal tissue. Solid areas are composed primarily of moderately cellular neural tissue with primitive neuroepithelial cells with frequent resetting and pigmentation resembling developing eye. Cysts are lined by a cuboidal epithelial cells.
SC11-014	Undifferentiated	14	ESC	++	+	++	-	Well differentiated pluripotent teratoma	Within the cut section of the tumor, there is benign well differentiated teratoma composed of solid and cystic areas and contain tissue types arising from all three primordial germ cell layers. Solid areas are composed of mixed population of moderately cellular neural tissue with glial cells and smaller primitive neuroepithelial cells in a background of neurofibrillary material. Additional solid areas include cartilage & muscle tissue. There are numerous cysts are lined by variety of cells ranging from simple columnar to stratified squamous epithelium. These cysts are vary from being respiratory tract epithelium to skin
SC11-014	Undifferentiated	14	ESC	+++	+	+++	-	Poorly differentiated teratoma	Within the cut section of the tumor, there is benign poorly differentiated teratoma composed of solid and cystic areas and contain tissue types arising from all three primordial germ cell layers. Solid areas are composed primarily of moderately cellular neural tissue with neurons, glial cells and smaller, primitive neuroepithelial cells in a background of neurofibrillary material. Additional solid tissue include cartilaginous tissue. Cysts are lined by a variety of epithelial cells, ranging from squamous to cuboidal to simple and pseudostratified columnar with multifocal cilia. Few to many goblet cells are present in some cysts. Some cysts contain eosinophilic to amphophilic amorphous to fibrillar material.

Table S9: Summary of files and accession numbers available in Synapse. Enter the accession number into the search field at www.synapse.org to access the resource.

Resource	Accession #
Study Homepage	syn1773109
Cell Line Descriptions	
Cell line Metadata	syn2767694
Sample/Assay Metadata Folder	syn2247883
Experimental Protocols	
Top-level folder	syn2512369
Cell thaw/plate protocol	syn2724705
PSC culture protocol	syn2724700
Embryoid Body differentiation protocol	syn2512370
Preliminary Screening	
Teratoma Reports	syn2882776
Teratoma Report Spreadsheet	syn2882785
Karyotype full reports	syn2679104
Data (Raw and Normalized, potential additions after publication)	
Top-level folder	syn1773110
RNA-seq raw data	syn2247098
Exon and junction bed files (RNA-seq)	syn2246520
Gene expression normalized data	syn3034437
Alternative splicing PSI data	syn3091916
miRNA-seq raw data	syn2247097
microRNA normalized data	syn2701942
DNA methylation raw data	syn2653626
DNA methylation normalized data	syn2233188
Taqman Low-Density Array (TLDA) data	syn3107327
SNP array clinical reports	syn2679103
Compiled CNV data and Excel graphs	syn3105726
Analysis Scripts and Results (frozen at publication)	
Scripts Top-level Folder	syn2246673
Methylation Normalization script	syn2677441
Covariate Analyses Top Level	syn3094629
Gene Expression Covariate Results	syn3106206
Alternative Splicing Covariate Results	syn3106266
DNA Methylation Covariate Results	syn3106255
microRNA Covariate Results	syn3106244
Alternative Splicing hESC vs EB results	syn3106284
Ancestry Analysis	syn3107098
AltAnalyze Sample Group Predictions	syn3107554
Other Documents	
Manuscript Homepage	syn2731183
Suppl - Xchr_methylation-RNASeq_anticorrelated.xlsx	syn3107536
Suppl - XchrNazor_methylation-RNASeq.xlsx	syn3107535